Red Blood Cell Susceptibility to Pneumolysin

Bokori-Brown, Monika; Petrov, Peter G; Khafaji, Mawya A; Mughal, Muhammad K; Naylor, Claire E; Shore, Angela C; Gooding, Kim M; Casanova, Francesco; Mitchell, Tim J; Titball, Richard W; Winlove, C Peter

DOI:
10.1074/jbc.M115.691899

THE JOURNAL OF BIOLOGICAL CHEMISTRY VOL. 291, NO. 19, pp. 10210–10227, May 6, 2016

Red Blood Cell Susceptibility to Pneumolysin

*CORRELATION WITH MEMBRANE BIOCHEMICAL AND PHYSICAL PROPERTIES**

Received for publication, September 14, 2015, and in revised form, February 23, 2016 Published, JBC Papers in Press, March 16, 2016, DOI 10.1074/jbc.M115.691899

Monika Bokori-Brown[‡1], Peter G. Petrov[§], Mawya A. Khafaji[§2], Muhammad K. Mughal[¶], Claire E. Naylor[‖], Angela C. Shore[‡‡], Kim M. Gooding[**‡‡], Francesco Casanova[**‡‡], Tim J. Mitchell[¶], Richard W. Titball[‡], and C. Peter Winlove[§]**

From the [‡]College of Life and Environmental Sciences, School of Biosciences, University of Exeter, Exeter EX4 4QD, United Kingdom, the [§]College of Engineering, Mathematics and Physical Sciences, School of Physics, University of Exeter, Exeter EX4 4QL, United Kingdom, the [¶]Institute of Microbiology and Infection, University of Birmingham, Birmingham B15 2TT, United Kingdom, the [**]Department of Diabetes and Vascular Medicine, University of Exeter Medical School, Barrack Road, Exeter EX2 5AX, United Kingdom, the [‡‡]National Institute for Health Research Exeter Clinical Research Facility, Royal Devon and Exeter National Health Service Foundation Trust, Exeter EX2 5DW, United Kingdom, and the [‖]Department of Biological Sciences, Birkbeck College, Malet Street, London WC1E 7HX, United Kingdom

This study investigated the effect of the biochemical and biophysical properties of the plasma membrane as well as membrane morphology on the susceptibility of human red blood cells to the cholesterol-dependent cytolysin pneumolysin, a key virulence factor of *Streptococcus pneumoniae*, using single cell studies. We show a correlation between the physical properties of the membrane (bending rigidity and surface and dipole electrostatic potentials) and the susceptibility of red blood cells to pneumolysin-induced hemolysis. We demonstrate that biochemical modifications of the membrane induced by oxidative stress, lipid scrambling, and artificial cell aging modulate the cell response to the toxin. We provide evidence that the diversity of response to pneumolysin in diabetic red blood cells correlates with levels of glycated hemoglobin and that the mechanical properties of the red blood cell plasma membrane are altered in diabetes. Finally, we show that diabetic red blood cells are more resistant to pneumolysin and the related toxin perfringolysin O relative to healthy red blood cells. Taken together, these studies indicate that the diversity of cell response to pneumolysin within a population of human red blood cells is influenced by the biophysical and biochemical status of the plasma membrane and the chemical and/or oxidative stress pre-history of the cell.

The interaction of toxins with their target cells is generally characterized by a dose-response curve that is sigmoidal in shape (1). This shape is taken to reflect the differing susceptibilities of individual cells within the population. The fact that red blood cells (RBCs), with their less developed glycocalyx compared with other cell types (2), exhibit such a response is evidence that the initial interaction between the toxin and the plasma membrane is subject to, and probably the main determinant of, such variability. Therefore, it is important to understand the biochemical and biophysical factors affecting toxin-membrane interactions and the resulting variability of susceptibility within the same cell population.

Individual RBCs within a population differ significantly (3) with respect to their shape, volume, and surface area. Some of these changes are related to cell age, due to the variety of mechanical and chemical stresses that an RBC undergoes in its life span of ~120 days (4, 5), and others can be associated with diseases, such as diabetes and with acute conditions, such as sepsis, among many others (6), and thus are likely to be present in the membranes of many other cell types.

Previous work on bulk cell preparations revealed that in addition to its normal discocytic shape, the RBC at rest can assume a variety of other distinct shapes, such as echinocytes and acanthocytes, characterized by exterior projections, and stomatocytes with cup-shaped invaginations (7). Many of these unusual shapes appear in normal blood at a frequency of about 1%. However, during blood bank storage and in many inflammatory, degenerative, and microvascular disorders, the frequency of RBCs with altered morphology increases (8–12). For example, an increase of 13% in echinocytes was observed in patients suffering from chronic hepatitis (13), and in neuroacanthocytosis syndromes, a group of rare neurodegenerative diseases that mainly affect children and young adults, acanthocytes appear with a frequency of 12–45% (14).

High heterogeneity in the size of circulating erythrocytes can also have a dramatic impact on the health and function of the entire cell population (4, 5, 15). Recent studies indicate that the RBC distribution width, a measure of the size variation of circulating erythrocytes with a normal reference range of 11–15% (16), is a strong predictor of cardiovascular and thrombotic disorders (15, 17), with a positive correlation between increased RBC distribution width and peripheral artery diseases (18).

Aging RBCs are characterized by a decrease in size, usually explained in terms of a decrease in cell area due to loss of lipids

* This work was supported by the Defence Science and Technology Laboratory Grant DSTLx1000075949, Porton Down, UK. The views expressed are those of the author(s) and not necessarily those of the National Health Service, the National Institute for Health Research (NIHR), or the Department of Health. The authors declare that they have no conflicts of interest with the contents of this article.

[1] To whom correspondence should be addressed: College of Life and Environmental Sciences, School of Biosciences, Geoffrey Pope Bldg., Stocker Rd., University of Exeter, Exeter EX4 4QD, UK. Tel.: 44-1392-725157; Fax: 44-1392-723434; E-mail: m.bokori-brown@exeter.ac.uk.

[2] Present address: Dept. of Radiology, School of Medicine, King Abdulaziz University, P. O. Box 80215, Jeddah 21589, Kingdom of Saudi Arabia.

(19), and by surface modifications that include external exposure of membrane phosphatidylserine (PS)[3] and decreased levels of sialic acid (20, 21). Exposure of PS on the outer leaflet of the membrane marks the cell for recognition and phagocytosis by macrophages.

A number of studies have shown that aging of RBCs influences their sensitivity to bacterial toxins. For example, human RBCs during blood bank storage become more susceptible to sublytic concentrations of phospholipase C from either *Bacillus cereus* or *Clostridium perfringens* (12, 22). Age-development changes in susceptibility of RBCs to the pore-forming toxin (PFT) perfringolysin O (PFO) from *C. perfringens*, a member of the cholesterol-dependent cytolysin (CDC) family of PFTs, have been demonstrated in mice, with RBCs of old mice being more susceptible to the toxin than those of young mice (23). Old RBC populations and peroxyl-oxidized RBCs also showed more susceptibility to hemolysis by the PFT stycholysin II from the sea anemone *Stichodactyla helianthus* compared with young cell populations (21). In contrast, old RBCs from rabbits are less susceptible to *Staphylococcus aureus* α-toxin relative to young RBCs (24–26). This is due to degradation of the membrane protein band 3 in older RBCs (27), a binding site for staphylococcal α-toxin. The chemistry of lipid rafts (*e.g.* cholesterol content) is also known to change with age, and such changes could alter the susceptibility of the host cell to toxic action (28).

Like PFO, pneumolysin (PLY) is also a member of the CDC family of PFTs (29). PLY is a key virulence factor of the bacterial pathogen *Streptococcus pneumoniae* (30, 31) and plays a role in a range of human diseases, such as pneumonia, sepsis, and meningitis (32). Disease is especially common in children, the elderly, and in immunocompromised and diabetic individuals (30).

PLY is released from the bacterium as an inactive water-soluble monomer (53 kDa). Monomeric PLY is an elongated molecule organized into four domains (33, 34). Three short hydrophobic loops and the highly conserved tryptophan-rich loop at the base of domain 4 anchor the toxin to the membrane (35, 36), with a highly conserved threonine-leucine pair in loop 1 critical for cholesterol binding (37), the receptor for most CDCs (38, 39). Two putative carbohydrate-binding sites have also been identified in PLY, one near the conserved tryptophan-rich loop in domain 4 and the other at the domain 3-domain 4 interface (33, 40).

Pore formation by PLY is a multistep process. Upon binding to the membrane, PLY monomers interact with each other and form an oligomeric pre-pore complex on the membrane surface that contains 30–50 monomers (41, 42). Pre-pore to pore transition is associated with significant conformational changes in the complex and consequent membrane insertion of the oligomer that leads to the formation of large pores of 32–43 nm in diameter and ultimately to cell lysis (43–45).

A wide range of host cells are susceptible to the action of PLY, and although erythrocytes are not the primary target for the toxin *in vivo*, they are the cell type most commonly used to measure activity toward host cells (46).

To date, the relationship between the plasma membrane properties and the variability in cell response to toxin within a population has largely been unexplored. Therefore, the aim of this study was to investigate the effect of the biochemical (oxidative stress, lipid scrambling, and artificial cell aging) and biophysical properties (bending rigidity and surface and dipole electrostatic potentials) of the plasma membrane and the effect of membrane morphology on the susceptibility of RBCs to PLY (47), using single cell studies. Finally, we sought to establish whether the response to PLY in populations of RBCs derived from diabetic subjects correlates with levels of glycated hemoglobin (Hba1c), which is elevated in people with diabetes and is likely to alter membrane physical characteristics via glucose-induced biochemical modifications.

Experimental Procedures

Materials—Chemicals were purchased from Sigma, UK, unless otherwise stated. Recombinant wild-type pneumolysin with an N-terminal His_6 tag (PLY) and recombinant wild-type pneumolysin with an N-terminal His_6 and eGFP tags (eGFP-PLY) and PFO were generated, expressed, and purified as described previously (48–50); eGFP-PLY is monomeric in solution as judged by size exclusion chromatography and analytical ultracentrifugation experiments and has a specific activity similar to unlabeled PLY at equivalent molarity (data not shown). Recombinant plasmid pET-33b(+) containing the non-lytic and aggregation-negative variant of eGFP-PLY, termed eGFP-Δ6PLY^{L363A}, was generated as described previously (49).

Expression and Purification of eGFP-Δ6PLY^{L363A}—For expression of eGFP-Δ6PLY^{L363A}, recombinant plasmid was transferred into *Escherichia coli* Rosetta 2 (DE3) cells (Merck, Darmstadt, Germany), and expression of eGFP-Δ6PLY^{L363A} was induced using the autoinduction system as described previously (51).

Time Course of Hemolysis Induced by PLY within a Population of Human RBCs—Fresh whole blood from healthy ($n = 17$) and diabetic individuals ($n = 36$) was collected by venipuncture from the University of Exeter Medical School, National Institute for Health Research Exeter Clinical Research Facility, Diabetes and Vascular Medicine Centre, Exeter, UK,[4] into neutral tubes, and 1 ml of whole blood was immediately transferred into 20 ml of DPBS buffer, pH 7.0–7.2 (Invitrogen), supplemented with 1 mg/ml bovine serum albumin (BSA) (DPBS/BSA). RBCs were washed three times in DPBS/BSA, resus-

[3] The abbreviations used are: PS, phosphatidylserine; PFT, pore-forming toxin; PLY, pneumolysin; PFO, perfringolysin O; CDC, cholesterol-dependent cytolysin; RBC, red blood cell; DPBS/BSA, DPBS buffer, pH 7.0–7.2, supplemented with 1 mg/ml bovine serum albumin; cumOOH, cumene hydroperoxide; DHEA, dehydroepiandrosterone; FPE, fluorescein-phosphatidylethanolamine; eGFP, enhanced green fluorescent protein; H_2O_2, hydrogen peroxide; Hba1c, glycated haemoglobin; DIC, differential interference contrast.

[4] Ethical approval was granted by the National Ethics Research Service South West-Exeter Research Ethics Committee, Reference 10/H0206/67. Human blood samples obtained from the University of Exeter Medical School, National Institute for Health Research Exeter Clinical Research Facility, Diabetes and Vascular Medicine Centre, Exeter, UK, were processed in the National Institute for Health Research Exeter Clinical Research facility following written informed consent by all participants.

pended in DPBS/BSA at a concentration of 3×10^7 cells/ml, and cells (90 μl) were incubated with PLY at a final concentration of 118 ng/ml (2.2 nM) for 30 min at room temperature, similar to the dose (1 nM) frequently used in the literature under comparable experimental conditions (40, 52). The time course of hemolysis was monitored by phase contrast microscopy (Zeiss Axiophot upright microscope equipped with a Plan Neofluar ×20/0.5 air objective). Images were captured every 2 min for 30 min using a Spot Pursuit™ 1.4 MP monochrome CCD camera (Visitron Systems). The number of lysed cells was counted, and the percentage of lysed cells was calculated for each time point.

Analysis of Binding of Recombinant eGFP-PLY and eGFP-Δ6PLY^{L363A} to Human RBCs by Microscopy—To investigate whether the variation of cell response to PLY within a population of RBCs correlates to the amount of toxin bound to the membrane, RBCs (Innovative Research) were diluted to 6×10^7 cells/ml in DPBS/BSA, and cells (90 μl) were incubated with eGFP-PLY at a final concentration of 0.67 μg/ml to allow optimal detection of eGFP fluorescence by microscopy.

To investigate whether increased sensitivity of stomatocytes to PLY correlates to the amount of toxin bound to the membrane, fresh blood was collected from healthy volunteers using a pin-prick lancet and immediately suspended in DPBS/BSA ($\sim 3 \times 10^7$ cells/ml). Cells (90 μl) were incubated with eGFP-Δ6PLY^{L363A} at a final concentration of 1.12 μg/ml.

Cells were imaged at room temperature using an Olympus IX81 microscope (Olympus Optical, Hamburg, Germany) equipped with a PlanApo ×100/1.40 oil objective and eGFP filter sets equipped with a 470/40 ET bandpass filter, beam splitter T 495 LPXR, and a 525/50 ET bandpass filter (Chroma Technology Corp., Olching, Germany).

Each image had its background intensity subtracted, and the GFP intensities of cells were measured 2 min after exposure to toxin using ImageJ software (53).

Simulated Oxidative Stress and Aging—Fresh whole blood from healthy individuals was collected by venipuncture from the University of Exeter Medical School, National Institute for Health Research Exeter Clinical Research Facility, Diabetes and Vascular Medicine Centre, Exeter, UK, into neutral tubes and 1 ml of whole blood was immediately transferred into DPBS/BSA. Cells were washed three times with DPBS/BSA and resuspended in DPBS/BSA to 3×10^7 cells/ml.

To simulate oxidative stress, we used two different oxidants, the water-soluble hydrogen peroxide (H_2O_2) and the membrane-soluble cumene hydroperoxide (cumOOH). Solutions were prepared in DPBS/BSA immediately before each experiment to minimize peroxide degradation. To disperse cumOOH at the necessary concentration into DPBS/BSA, the mixture was vigorously vortexed for a few minutes.

We used two different approaches to simulate cell aging. The first one relies on cell treatment with the steroid hormone dehydroepiandrosterone (DHEA). In DHEA-treated cells, inhibition of glucose-6-phosphate dehydrogenase activity resulted in decreased levels of NADPH, an essential cofactor that helps maintain glutathione (GSH) in its reduced antioxidant form (54). Thus, decreased levels of GSH weaken the cell's antioxidant defense system. The second approach used calcium ionophore A23187. It has been demonstrated that treatment of RBCs with calcium ionophore A23187 causes internalization of Ca^{2+} leading to fast PS translocation from the inner monolayer to the outer monolayer of the plasma membrane, as well as cell shrinkage and membrane blebbing, which are typical signs of apoptosis (55–58).

Human RBCs from healthy individuals were diluted to 3×10^7 cells/ml in DPBS/BSA, and cells (1 ml) were incubated with H_2O_2 (100 μM), cumOOH (100 μM), DHEA (35 μM), calcium ionophore A23187 (20 μM, in the presence of 0.9 mM calcium chloride), or DPBS/BSA (as control) for 2 h at 37 °C. The solvent concentration in DHEA and calcium ionophore A23187-treated samples was kept below 1% (v/v). After incubation, cells were washed three times in DPBS/BSA and resuspended in 1 ml of DPBS/BSA. Cells (90 μl) were exposed to PLY at a final concentration of 118 ng/ml or perfringolysin O at a final concentration of 72 ng/ml, and the time course of hemolysis was monitored by phase contrast microscopy (Zeiss Axiophot upright microscope equipped with a Plan Neofluar ×20/0.5 air objective). Images were captured every 2 min for 30 min using a Spot Pursuit™ 1.4 MP Monochrome CCD camera (Visitron Systems). The number of lysed cells was counted, and the percentage of lysed cells was calculated for each time point.

Flow Cytometry Analysis of Calcium Ionophore A23187-treated RBCs Exposed to eGFP-Δ6PLY^{L363A}—Human RBCs from healthy individuals were diluted to 5×10^6 cells/ml, and cells (1 ml) were incubated with calcium ionophore A23187 (20 μM, in the presence of 0.9 mM calcium chloride) or ethanol aqueous solution (as control) for 1 h at 37 °C; the solvent (ethanol) concentration in both samples was 0.1% (v/v). After incubation, cells were washed three times in DPBS/BSA and resuspended in annexin V binding buffer (10 mM HEPES, 140 mM sodium chloride and 2.5 mM calcium chloride, pH 7.4, BD Biosciences) at a concentration of 1×10^6 cells/ml. Cells (100 μl) were labeled with 5 μl annexin V Alexa Fluor® 594 Conjugate (Molecular Probes) for 15 min at room temperature followed by incubation with eGFP-Δ6PLY^{L363A} at a final concentration of 1.67 μg/ml for 2 min at room temperature. After the incubation period, 400 μl of ice-cold annexin V binding buffer was added to each sample, and cells were analyzed by flow cytometry using 488 and 633 nm excitation on a BD FACSARIA II cytometer (BD Biosciences) with 530/30 and 660/20 bandpass filters. The number of events noted for each sample was 10,000.

Ratiometric Measurement of the Membrane Dipole Potential—In separate experiments, the membrane dipole potential was measured before exposing RBCs (100 μl at 3×10^7 cells/ml in DPBS/BSA) to PLY (5.9 ng/ml) in a μ-Slide I$^{0.4}$ Luer poly-L-lysine imaging chamber (Ibidi). The membrane dipole potential was measured using ratiometric fluorescence imaging of Di-8-ANEPPS-labeled RBC membranes. 5 μl of 1 mg/ml Di-8-ANEPPS in ethanol was added to 1 ml of RBC suspension, and cells were incubated at 37 °C for 1 h. Subsequently, cells were washed three times in DPBS/BSA to remove excess dye and resuspended in 1 ml of DPBS/BSA. Ratiometric measurement of the membrane dipole potential was performed on an Olympus IX50 inverted microscope using a ×63 oil immersion objective. Excitation light with a selectable wavelength was pro-

vided by a Till Photonics Polychrome V monochromator, and the images were recorded using a high sensitivity CCD camera (AVT Stingray F-145B) attached to the microscope in conjunction with a 650/50 nm emission filter (Thorlabs). Two consecutive images using excitation at 420 and 520 nm (each with an exposure time of 500 ms, with 5 ms between them) were recorded. Each image ($n = 24$) had its background intensity subtracted before the 420-nm excitation image was divided by the 520-nm excitation image to produce a matrix of the ratiometric intensity, $r = I_{420}/I_{520}$ using ImageJ software (53). The value of the membrane dipole potential ψ_d (in mV), averaged over the whole cell, can be found from the following calibration dependence (59) shown in Equation 1,

$$\psi_d = \frac{R + 0.3}{0.0043} \quad \text{(Eq. 1)}$$

Measurement of the Membrane Surface Potential—Similarly to the membrane dipole potential, the membrane surface electrostatic potential of RBCs (100 μl at 3×10^7 cells/ml in DPBS/BSA) was evaluated before exposing the cells to PLY (5.9 ng/ml) in a μ-Slide I$^{0.4}$ Luer poly-L-lysine imaging chamber (Ibidi). The membrane surface potential was measured using fluorescence intensity measurements of fluorescein-phosphatidylethanolamine (FPE; Molecular Probes) incorporated in the RBC membrane. The quantum yield of this probe is sensitive to the charge density of its immediate environment. Therefore, changes in the membrane surface electrostatic potential are manifested by changes in the fluorescence intensity recorded (60, 61). A decrease in the net negative charge of the surface results in deprotonation of fluorescein and a consequent increase in its fluorescence intensity.

Human RBCs were labeled with FPE following a protocol adapted from Ref. 62. In brief, 12.5 μg of FPE dissolved in 2.5 μl of ethanol was added to 3×10^7 RBCs in 1 ml of DPBS/BSA, and cells were incubated at 37 °C for 1 h. Subsequently, cells were washed three times in DPBS/BSA to remove excess dye and resuspended in 1 ml of DPBS/BSA. Fluorescence intensity measurements of FPE-labeled cells ($n = 108$) were performed using an Olympus IX81 microscope (Olympus Optical, Hamburg, Germany) equipped with a UPlanFL N ×40/1.3 oil objective and eGFP filter sets equipped with a 470/40 ET bandpass, beam splitter T 495 LPXR and a 525/50 ET bandpass filter (Chroma Technology Corp.).

Measurement of the Membrane Bending Elasticity Using Thermal Fluctuation Spectroscopy—Human RBCs were also interrogated for their mechanical properties, in particular membrane bending elasticity, using thermal fluctuation spectroscopy as described in more detail earlier (63, 64). In brief, individual RBCs ($n = 9$) were recorded using phase contrast microscopy (Leica DMLFS upright microscope equipped with ×63 PL Fluotar objective). Video sequences (about 1000 frames) of fluctuating RBCs were recorded at an exposure time of 10 ms using a QImaging QIClick CCD camera attached to the microscope and interfaced with a computer, and each frame was analyzed by a sub-pixel precision algorithm to obtain a series of two-dimensional equatorial contours. Each contour was decomposed into a Fourier series used subsequently to calculate the thermal fluctuation spectrum of the entire contour sequence as described previously (63, 64). The bending elastic modulus of the membrane was obtained by fitting a flat membrane model to the experimentally obtained thermal fluctuation spectrum (a full discussion of the bases of this methodology can be found in Ref. 64). For these experiments, 5-μl samples of fresh blood was collected from a healthy volunteer using a pinprick lancet and immediately suspended in 1 ml of DPBS/BSA. A small volume (~20 μl) of this suspension was introduced in an imaging chamber that consisted of a microscope slide and a glass coverslip spaced apart by two strips of Parafilm® (Pechiney Plastic Packaging) along the long edges of the slide, bonded together by heating briefly on a hot plate. Within a few minutes, the cells settle down onto the bottom of the chamber (due to their slightly higher density than that of the surrounding buffer), which allowed their fluctuations to be recorded before introducing the toxin solution (DPBS/BSA containing PLY at a final concentration of 59 ng/ml) by placing excess solution on one side of the chamber and pulling it through with filter paper introduced to the opposite side.

Monitoring the Changes in the Radius of RBCs Exposed to PLY Over Time—Changes in the radius of the equatorial contour of RBCs are an indicator for the onset of lysis. Therefore, we measured the radius of individual cells before and after introducing the toxin solution into the imaging chamber using the same methodology as for the thermal fluctuation analysis (in fact, radius evaluation is a part of the Fourier representation of the contour). In all experiments, cell membrane radii were initially recorded while in DPBS/BSA after the cells have stabilized on the bottom of the chamber. The buffer was then exchanged with buffer containing PLY (59 ng/ml), and RBCs were recorded at regular time intervals (typically every 2 min for a period of up to 30 min).

Measurement of Hba1c Levels in RBCs from Diabetic Individuals—Levels of glycated hemoglobin (HbA1c) were determined with the Gold Standard Ion-Exchange method using the Tosoh G8 HPLC Analyzer (Tosoh Bioscience, South San Francisco).

Measurement of the Modulus of Shear Elasticity—To measure the RBC shear elastic modulus, we employed the micropipette aspiration method. In brief, a micropipette is brought in close proximity to a cell, which is then partially aspirated into the pipette by applying small suction pressure. Subsequent incremental increases in the suction pressure leads to a stepwise aspiration of the cell membrane into the pipette, which allows the establishment of the relationship between the applied suction pressure, ΔP, and the projected length of the membrane inside the pipette, L. The shear elastic modulus, μ, can then be evaluated from such dependences according to Equation 2 (65, 66),

$$\Delta P R_p = \mu\left(K_1\left(\frac{L}{R_p}\right) - K_2\right) \quad \text{(Eq. 2)}$$

where R_p is the pipette radius, and $K_1 = 2.45$ and $K_2 = 0.603$ are numerical constants. Equation 2 is valid for $1 \leq L/R_p \leq 4$.

Micropipettes were drawn from glass capillaries of 0.86 mm internal diameter (Harvard Instruments GC 150-11)

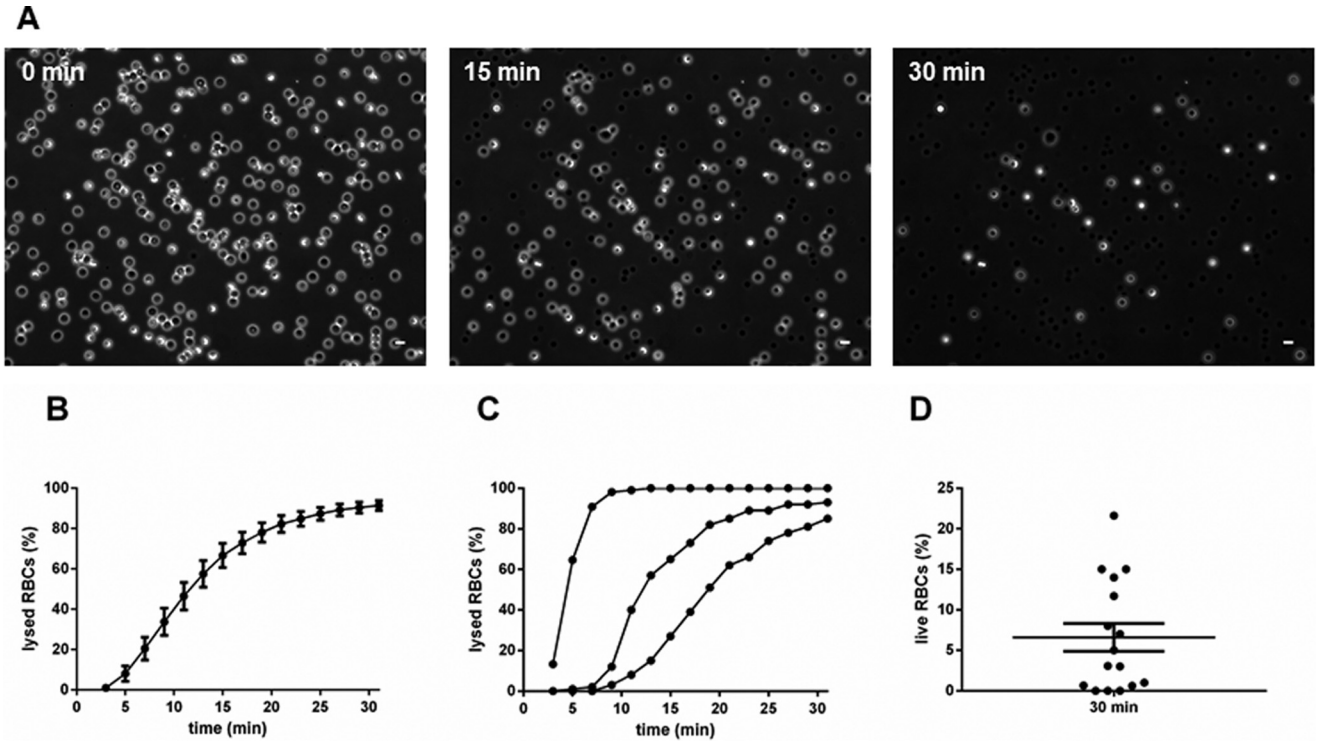

FIGURE 1. **Variation of RBC response to PLY.** *A*, representative phase contrast images of RBCs exposed to PLY. *Scale bar*, 5 μm. *B*, average ($\pm$ S.E.) time course of hemolysis induced by PLY (118 ng/ml) in RBCs from 17 healthy individuals. *C*, individual time courses of hemolysis induced by PLY (118 ng/ml) in RBCs from three healthy individuals. *D*, dot plot of the percentage of live RBCs 30 min after exposure of RBCs from 17 healthy individuals to PLY (118 ng/ml).

using a microelectrode puller (Micro Instruments Ltd., Oxford, UK). The end of the pipette was then manually forged with a heated filament until a smooth aperture was produced with typical diameters of 1–2 μm. The pipette was filled with buffer and attached to a pressure-generating apparatus capable of controlling the suction pressure via careful adjustments of the height of a buffer reservoir. The micropipette was then mounted on a hydraulically driven micromanipulator (Narishige Co. Ltd.) and its tip was introduced into the chamber containing the cell suspension. Images were acquired using a Leica DMLFS upright microscope ($\times$40 long working distance objective), a video camera (JVC KY-F55B), and acquisition software (AcQuis Bio 3.01).

The University of Exeter Medical School, National Institute for Health Research Exeter Clinical Research Facility, Diabetes and Vascular Medicine Centre, provided blood samples from individuals with diabetes ($n = 12$) and healthy ($n = 14$) subjects, stored at 4 °C in 9.5-ml heparinized tubes and used within 48 h. The individuals with diabetes were males over the age of 45 with no known diabetic complications and neither on insulin nor on metformin therapy. Control samples were obtained from age-matched healthy subjects.

Statistical Analyses—The software GraphPad Prism 6 (GraphPad Software, La Jolla, CA) was used to perform statistical analysis. In all analyses, p values of < 0.05 were considered significant. All data represent the means and standard deviations of three independent experiments performed in triplicate, unless stated otherwise.

Results

Variation of Response to Pneumolysin within a Population of Human RBCs—In the initial experiments, we sought to establish the behavior of human RBC populations in response to PLY. Fresh RBCs from healthy individuals ($n = 17$) were incubated with purified recombinant PLY (118 ng/ml), and the time course of hemolysis induced by the toxin on individual cells within each population was monitored by phase contrast microscopy. Fig. 1*A* shows representative phase contrast images of a population of RBCs exposed to PLY at time points 0, 15, and 30 min. In phase contrast, lysed cells appear as dark circles, whereas live cells appear with a distinctive halo around their edges. Fig. 1*B* shows the average ($\pm$ S.E.) hemolysis time profiles of 17 different donations treated with PLY. As evident from these results, the interaction between RBCs and PLY is characterized by a sigmoidal curve, which suggests a considerable degree of variability in the RBC response. At the toxin concentration used, a lag phase of ~3 min (on average) was followed by lysis where most cells were lysed by 30 min. Experiments carried out in the absence of PLY did not show any noticeable changes in the number of live cells on the time scale of the assay (data not shown).

To characterize the variability of RBC response to PLY within the same population, we compared the lysis behavior of RBCs exposed to PLY for each of the 17 individual samples. Fig. 1*C* shows three representative individual hemolysis time profiles from different healthy individuals. It can be seen that, although all samples exhibit the characteristic S-shaped curve, there are considerable quantitative variations between the indi-

vidual populations. Fig. 1*D* shows a dot plot of the percentage of live RBCs from 17 healthy individuals 30 min after exposure to PLY, where on average 6.6 ± 1.7% (S.E.) of RBCs remain resistant to PLY-induced lysis, despite all cells having been subjected to the same concentration of toxin.

Another important observation illustrated in Fig. 1*C* is the considerable degree of variability of RBC response to PLY within the same population, in which the time scale for cell lysis could differ by many minutes, despite the fact that all cells were derived from the same individual. To further investigate the variation of response to PLY within a population of RBCs, we monitored the changes in the radius of RBCs exposed to PLY over time. This revealed two distinct stages of interaction (Fig. 2). In the first stage (lasting different periods for different cells) the radius remains relatively constant. This is followed by a rapid drop in the radius in the second stage of interaction that corresponds to cell lysis. Fig. 2 shows typical time courses of the radius change for two RBCs from the same sample exposed to PLY, where the onset of cell lysis, marked by *arrows*, differs between the two cells by some 21 min. These results prompted us to further investigate the factors that influence the diversity of response to PLY within a population of cells. The experiments that follow were designed to address this question.

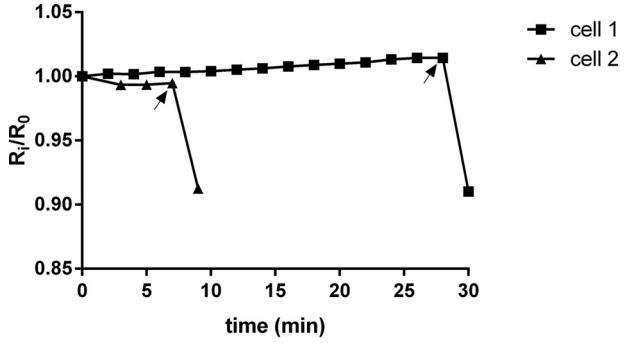

FIGURE 2. **Time dependence of the normalized contour radii for two cells from the same population exposed to PLY (59 ng/ml).** The radii at each time point (R_i) are normalized with respect to the values before the addition of toxin (R_0). *Arrows* indicate the onset of cell lysis.

Variation of Response to PLY within a Population of Human RBCs Correlates with the Amount of Toxin Bound to the Membrane—To investigate whether there is a correlation between the RBC response to PLY and the amount of toxin bound to the membrane, we incubated RBCs with recombinant GFP-tagged PLY (eGFP-PLY). Fig. 3*A* shows representative DIC and GFP fluorescence images obtained after exposure of RBCs to eGFP-PLY (0.67 μg/ml). The GFP fluorescence intensity of cells (n = 38) was measured 2 min after exposure to toxin. Most cells exposed to the toxin lysed within 2 min of exposure, indicated by the appearance of faint circles in the DIC image. However, some cells showed prolonged resistance to the toxin and in the DIC image appeared with a halo around their edges. Statistical analysis using Student's t test revealed that cells with prolonged resistance to the toxin showed significantly lower GFP fluorescence intensity values compared with cells that lysed within 2 min of exposure to toxin, indicating that variation of cell response to PLY within a population of RBCs correlates with the amount of toxin bound to the membrane (Fig. 3*B*). The punctate pattern of fluorescence on the RBC membrane probably corresponds to high molecular weight aggregates of the GFP-labeled toxin in the form of close-packed pores that have also been observed for the small β-PFTs, lysenin and ϵ-toxin (67–69). The pores can also be observed by analytical ultracentrifugation of membranes solubilized from toxin-treated cells or by electron microscopy (data not shown).

Effect of Cell Morphology on Susceptibility of RBCs to PLY—To investigate the effect of cell morphology on the susceptibility of RBCs to PLY, RBCs from 17 healthy individuals were incubated with PLY, as described above, and lysis was monitored by phase contrast microscopy. The shape of RBCs in each population was assessed using ImageJ, and the percentage of lysed discocytes and stomatocytes 15 min after exposure to PLY was determined (Fig. 4*A*). Statistical analysis using Mann-Whitney t test revealed that stomatocytes are more susceptible to PLY relative to discocytes, indicated by increased percentage of lysed cells 15 min after exposure to toxin (Fig. 4*A*).

To investigate whether the increased sensitivity of stomatocytes relative to discocytes correlates with increased levels of toxin bound to the membrane, we incubated live RBCs with

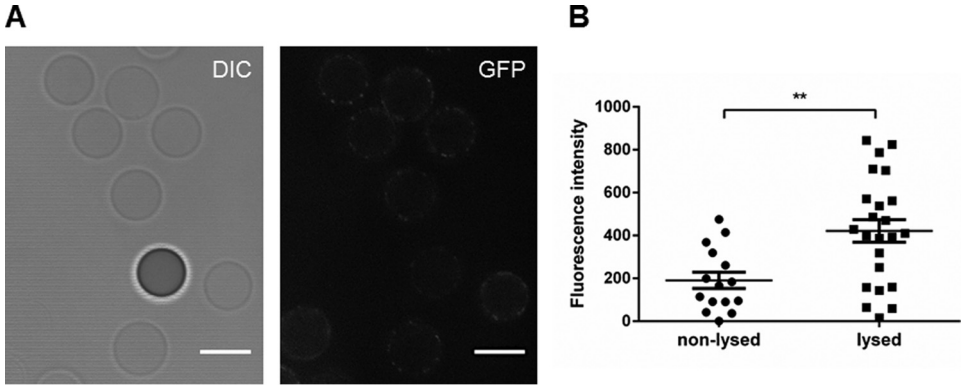

FIGURE 3. **Human RBCs with prolonged resistance to eGFP-PLY show reduced toxin binding.** *A,* representative DIC (*left*) and GFP fluorescence (*right*) images of RBCs incubated with eGFP-PLY (0.67 μg/ml). Lysed cells in the *left image* are characterized with faint outlines of their membranes. The cell with prolonged resistance to eGFP-PLY appears with a *halo* around its edge. *Scale bar,* 5 μm. *B,* correlation between GFP fluorescence intensity (hence eGFP-PLY concentration) on the surface of lysed and non-lysed cells. Each image had its background intensity subtracted, and the GFP intensities of cells (n = 38) were measured 2 min after exposure to toxin using ImageJ software (53). Significant differences are indicated: p = 0.0028 (**), unpaired, two-tailed Student t test.

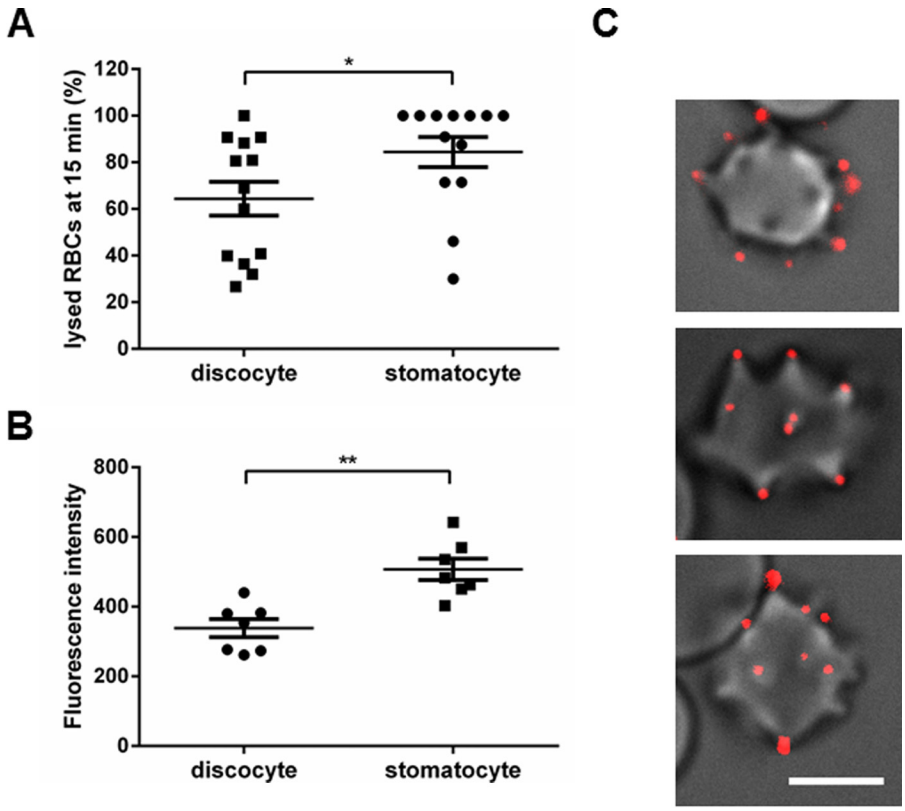

FIGURE 4. **Effect of cell morphology on the susceptibility of human RBCs to PLY.** *A,* RBCs from 17 healthy individuals were incubated with PLY (118 ng/ml), and the percentage of lysed discocytes and stomatocytes in each population was determined after exposure to PLY for 15 min. Significant differences are indicated: $p = 0.0211$ (*), unpaired, two-tailed Mann-Whitney *t* test. *B,* GFP fluorescence intensity of stomatocytes ($n = 7$) and discocytes ($n = 7$) after exposure to eGFP-Δ6PLY^{L363A} (1.12 μg/ml) for 2 min. Each image had its background intensity subtracted, and the GFP intensities of cells were measured using ImageJ software (53). Significant differences are indicated: $p = 0.0012$ (**), unpaired, two-tailed Mann-Whitney *t* test. *C,* merged DIC and GFP fluorescence images of echinocytes showing the distribution of eGFP-Δ6PLY^{L363A} on the surface of the cell. The fluorescence from eGFP-Δ6PLY^{L363A} is shown in *red*. *Scale bar,* 5 μm.

eGFP-Δ6PLY^{L363A}, a non-lytic variant of recombinant eGFP-PLY with preserved binding activity (49). As shown in Fig. 4*B*, stomatocytes showed significantly higher GFP fluorescence intensity values compared with discocytes.

In a separate group of experiments, we performed DIC and fluorescence imaging of echinocytic RBCs (formed spontaneously in the blood sample) incubated with eGFP-Δ6PLY^{L363A} (1.67 μg/ml) for 2 min. As can be seen from Fig. 4*C*, we observed clusters of eGFP-Δ6PLY^{L363A} bound preferentially to the spikes of the echinocytes, where the curvature of the membrane is high.

Simulated Oxidative Stress, Artificial Aging, and Membrane Lipid Scrambling of RBCs Leads to Changes in Susceptibility to PLY—To determine whether the variation of cell response to PLY might be due to differences in the biochemical status of the RBC membrane, we selectively modified the membrane using four different treatments. Oxidative stress was simulated by exposing RBCs to either hydrogen peroxide (H_2O_2, 100 μM) or cumOOH (100 μM). These two oxidants were used to selectively target different cell constituents. Hydrogen peroxide is water-soluble, and upon addition to the cell suspension it permeates the plasma membrane relatively quickly and partitions in the cytoplasm, thus targeting mainly hemoglobin (64, 70). In contrast, cumOOH is membrane-soluble and partitions predominantly into the lipid bilayer due to its hydrophobicity, where it is able to cause oxidative damage to lipids as well as to membrane-bound proteins and to the membrane skeleton (64, 70). To simulate aspects of the aging process in RBC, we exposed cells to the steroid DHEA (35 μM), as described under "Experimental Procedures." In a separate series of experiments, membrane lipid scrambling was induced using calcium ionophore A23187 (20 μM) in the presence of calcium chloride (0.9 mM).

Fig. 5 is a representative summary of the obtained results, along with a control of untreated cells. The typical sigmoidal response is observed again. However, there are considerable quantitative differences between the different treatment protocols. Treatment with H_2O_2 had no effect on the sensitivity of RBCs to PLY (the hemolysis profile in this case was similar to the control sample), although cumOOH-induced oxidative stress resulted in increased resistance to PLY relative to control cells, indicated by the low percentage of lysed cells over the time course of the experiment (30 min). A similar effect was observed in cells treated with calcium ionophore A23187. In contrast, artificially aged cells treated with DHEA exhibited higher susceptibility to PLY relative to control cells, indicated by the increased percentage of lysed cells over the time course of the experiment.

Increased Resistance of Calcium Ionophore A23187-treated RBCs to PLY Corresponds to Reduced Toxin Binding—The drastic changes in membrane lipid composition and loss of asymmetry between the two leaflets of the RBC membrane induced

by the calcium ionophore A23187 treatment required further investigation to assess the binding affinity of PLY to scrambled membranes. First, we labeled calcium ionophore A23187-treated and control RBCs with AlexaFluor® 594-annexin V. Because annexin V binds to PS, the expectation was that only cells in which PS is transferred to the outer membrane leaflet will become labeled with annexin V (for healthy RBCs PS is exclusively located in the inner membrane leaflet). These preparations were then incubated with either eGFP-Δ6PLY^{L363A} or buffer only, and toxin binding was analyzed by flow cytometry.

The first group of experiments was carried out on annexin V-labeled cells treated with calcium ionophore A23187 or ethanol aqueous solution (as control) before exposure to toxin. Flow cytometry analysis of dot plots that reflect cell shape revealed that calcium ionophore A23187-treated cells had altered cell morphology relative to control cells, with reduced forward scatter, indicating reduced size, and a narrow range of side scatter, indicating echinocytic morphology (Fig. 6*A*) (71).

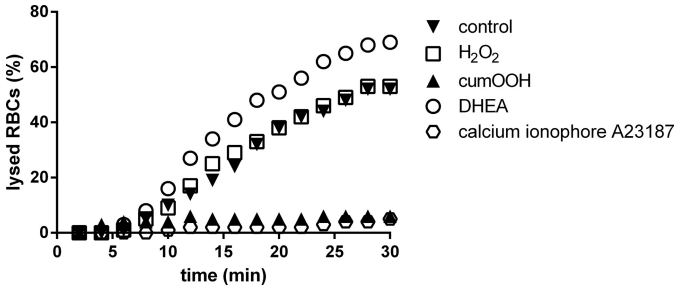

FIGURE 5. **Hemolysis profiles of a population of human RBCs that has undergone different biochemical treatments: ▼, control; □, H_2O_2; ▲, cumOOH; ○, DHEA; ○, calcium ionophore A23187.** One representative experiment out of three is shown.

Further microscopy analysis revealed projections of the cell membrane in calcium ionophore A23187-treated cells, leading to echinocytes (Fig. 6*B*).

Fluorescence analysis of calcium ionophore A23187-treated cells revealed that 36.2% of cells were labeled with AlexaFluor® 594-annexin V (Fig. 7*B*, *bottom right panel*), indicating transfer of PS to the outer membrane leaflet, whereas control cells showed only background red fluorescence of 0.09% (Fig. 7*A*, *bottom right panel*), indicating that PS is located exclusively in the inner membrane leaflet.

The second group of experiments was carried out on annexin V-labeled control and A23187-treated RBCs after exposure to eGFP-Δ6PLY^{L363A}. Flow cytometry analysis of annexin V-labeled control cells exposed to eGFP-Δ6PLY^{L363A} showed green fluorescence in 99.5% of cells (Fig. 7*C*, *top left panel*), indicating eGFP-Δ6PLY^{L363A} binding to most cells. Annexin V-labeled calcium ionophore A23187-treated cells exposed to eGFP-Δ6PLY^{L363A} showed green fluorescence in 59.1% of cells (Fig. 7*D*, *top left panel*) and double fluorescence of green and red in 39.2% of cells (Fig. 7*D*, *top right panel*), indicating eGFP-Δ6PLY^{L363A} binding to RBCs with both externalized and non-externalized PS. However, double fluorescence plots of red and green fluorescence show that the green fluorescence intensity in annexin V-labeled calcium ionophore A23187-treated cells exposed to toxin is reduced in comparison with annexin V-labeled control cells exposed to toxin (*top left panels* of Fig. 7, *D* and *C*, respectively). This tendency is especially visible for calcium ionophore A23187-treated cells with externalized PS (Fig. 7*D*, *top right panel*). These results indicate that increased resistance of A23187-treated cells to PLY is most probably due to reduced toxin binding to membranes with scrambled lipids.

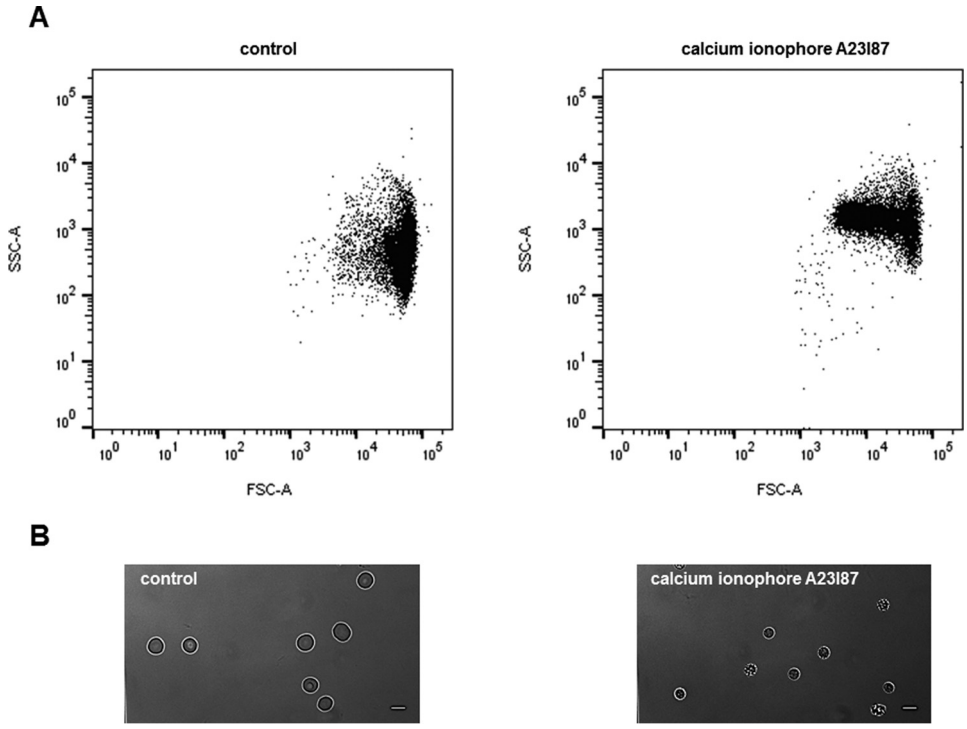

FIGURE 6. **Flow cytometry and phase contrast microscopy analysis of control and calcium ionophore A23187-treated human RBCs labeled with annexin V.** *A*, dot plots of side-scattered (*SSC-A*) *versus* forward-scattered (*FSC-A*) light. One representative experiment out of three is shown. *B*, representative phase contrast microscopy images of control and calcium ionophore A23187-treated RBCs. *Scale bar*, 5 μm.

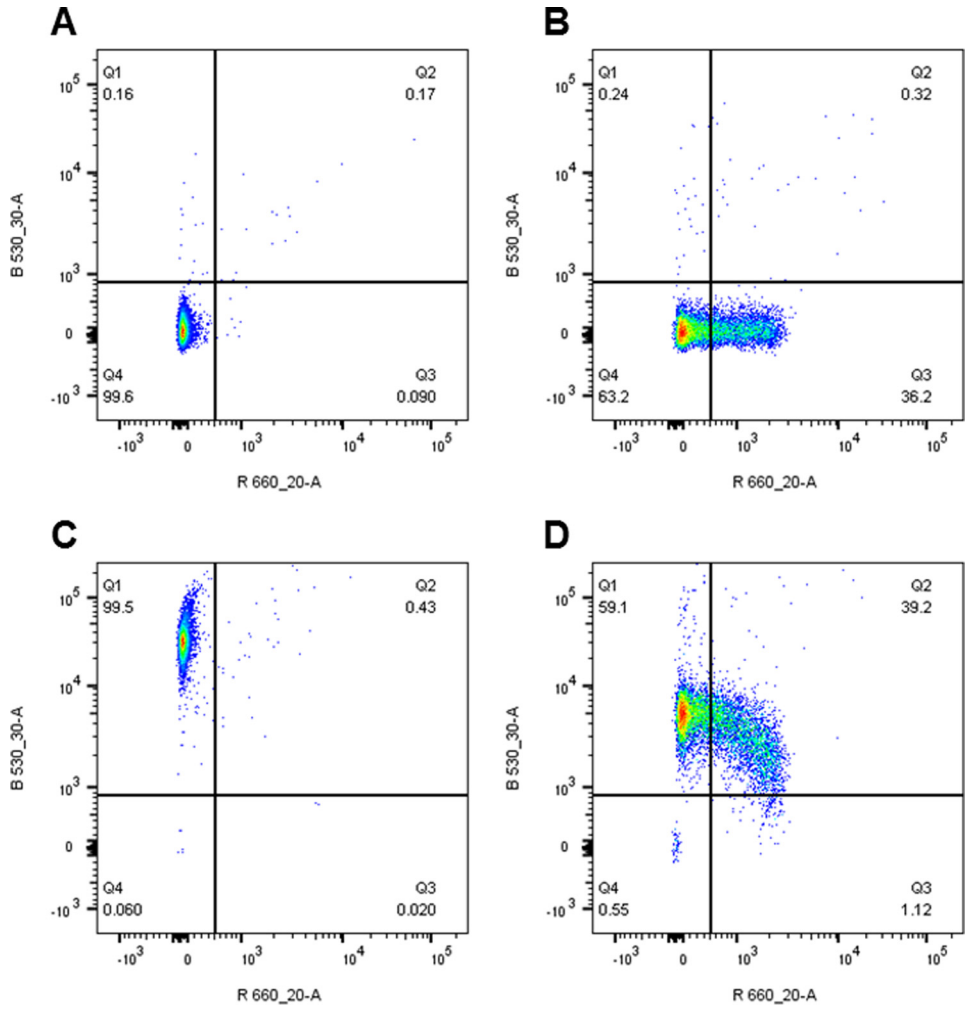

FIGURE 7. **Flow cytometry analysis of annexin V-labeled control and calcium ionophore A23187-treated RBCs before and after eGFP-Δ6PLY^{L363A} binding.** Double fluorescence plots of *red* ($Ex_{633\ nm}/Em_{650-670\ nm}$, annexin V) and *green* fluorescence ($Ex_{488\ nm}/Em_{515-545\ nm}$, eGFP-Δ6PLY^{L363A}) of control, before toxin (*A*), calcium ionophore A23187, before toxin (*B*); control, after toxin (*C*); and calcium ionophore A23187, after toxin (*D*). *Q1* = *green*; *Q2* = *green* and *red*; Q3 = *red*; Q4 = *not green* and *not red*.

Differences in the Membrane Physical Properties of Individual Cells within a Population of Human RBCs Are Correlated with Their Susceptibility to PLY—The physical properties of the lipid bilayer membrane, such as membrane elasticity and its electrostatic status, are likely determinants of the susceptibility of cells to toxin, as they have been shown to contribute to, as well as control, the interactions between the plasma membrane and various proteins (72–74). This motivated us to investigate whether differences in the membrane physical properties of individual cells within a population of RBCs are correlated with their susceptibility to PLY. We measured the membrane bending elastic modulus (a primary measure of the mechanical compliance of the lipid bilayer (75)), the membrane electrostatic dipole potential (76, 77), and the membrane electrostatic surface potential (60, 61) for a number of individual cells within a population of RBCs before toxin exposure. The buffer surrounding the cells was then exchanged with buffer containing toxin, and the time to lysis, *i.e.* the period of time the cell survived intact and without hemolysis after the addition of toxin, was monitored for each cell by microscopy.

Fig. 8*A* shows the dependence of the membrane bending elastic modulus (in units of k_bT, where k_b is the Boltzmann constant and T is the absolute temperature) on the time to lysis for nine individual cells. There is a clear correlation between these two parameters, where cells that are more rigid with respect to bending show reduced time to lysis, indicating increased susceptibility to the toxin's lytic activity.

In separate experiments, using ratiometric fluorescence microscopy measurements on Di-8-ANEPPS-labeled RBCs, we found a similar correlation between the membrane dipole potential and the time to lysis, as illustrated in Fig. 8*B*. Higher dipole potentials appear to be correlated with reduced time to PLY-induced lysis.

Finally, we measured the membrane-associated fluorescence intensity of FPE-labeled RBCs before toxin exposure to evaluate whether there is a correlation between the membrane electrostatic surface potential and the susceptibility of RBCs to PLY-induced lysis. Fig. 8*C* shows the measured membrane-associated fluorescence intensity as a function of time to lysis. Differences in the fluorescence intensity of FPE are indicative of the degree of natural variations in the magnitude of the surface electrostatic potential of the (negatively charged) RBC membrane. FPE is sensitive to changes in the surface potential due to a shift in the protonation-deprotonation equilibrium (61),

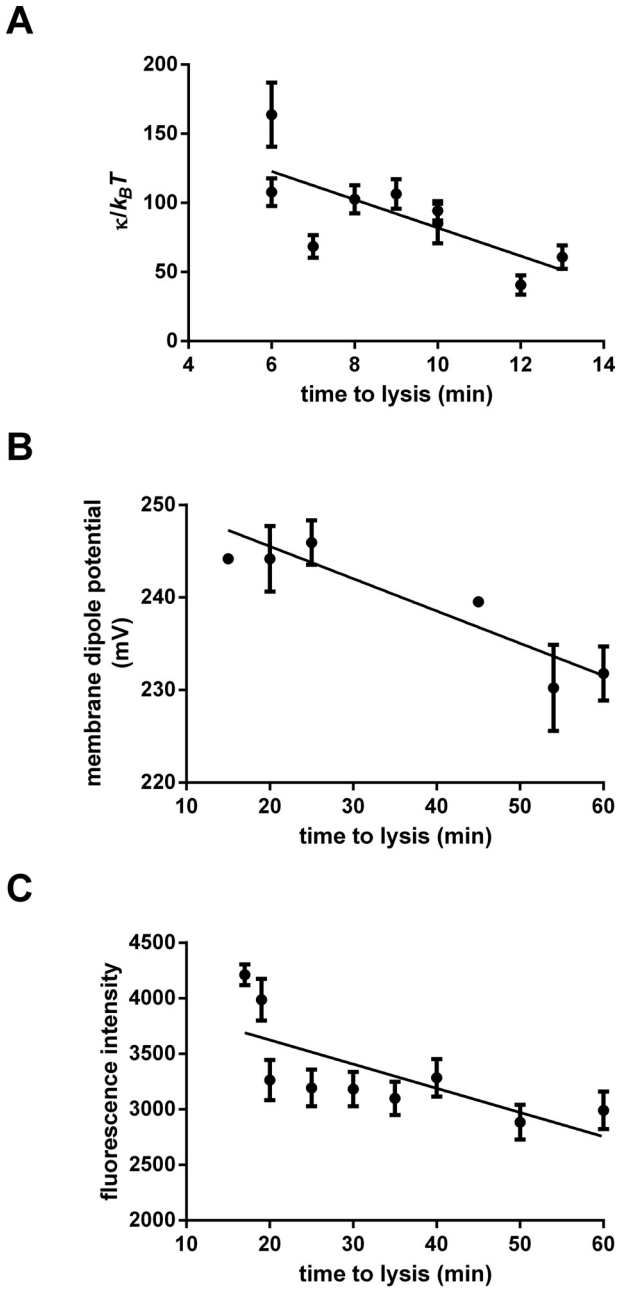

FIGURE 8. **Differences in the membrane physical properties of individual cells within a population of human RBCs are correlated with the susceptibility of cells to PLY.** *A,* dependence of the red blood cell membrane bending elastic modulus on the time to lysis. Cells ($n = 9$) were exposed to 59 ng/ml PLY. One representative experiment out of three is shown. Linear regression line, $R^2 = 0.52$, $p = 0.027$ (*). *B,* dependence of the RBC membrane dipole potential on the time to lysis. Cells ($n = 25$) were exposed to 5.9 ng/ml PLY. One representative experiment out of three is shown. Linear regression line, $R^2 = 0.40$, $p = 0.002$ (**). *C,* dependence of the measured fluorescence intensity of FPE-labeled RBCs on the time to lysis. Cells ($n = 108$) were exposed to 5.9 ng/ml PLY. One representative experiment out of three is shown. Linear regression line, $R^2 = 0.52$, $p = 0.029$ (*).

resulting in higher fluorescence intensities when the magnitude of the potential is lower. From these experiments we conclude that cells exhibiting a lower magnitude of the surface potential (hence lower surface density of negative charges) are more susceptible to toxin. Conversely, more negative membranes show increased resistance to lysis.

Correlation between Levels of Hba1c and Susceptibility of RBCs from Individuals with Diabetes to PLY—Next, we sought to establish whether the response to PLY in RBCs derived from diabetic subjects correlates with levels of Hba1c, which is elevated in diabetes; the higher the HbA1c levels, the greater the risk of developing diabetes-related complications. We investigated samples from 36 individuals (23 of whom were on metformin therapy, whereas 13 were not) for RBC susceptibility to PLY-induced lysis. Diabetic RBCs were exposed to PLY (118 ng/ml), and the percentage of live cells after exposure to toxin for 30 min was plotted against Hba1c levels. For the subset of individuals who were not treated with metformin (Fig. 9*A*), there is a statistically significant positive correlation between the percentage of live cells and Hba1c levels, indicating that RBCs from individuals with diabetes with increased levels of Hba1c are more resistant to PLY. For the other subset (individuals to whom metformin was prescribed), this correlation was much weaker, making the dependence statistically insignificant (Fig. 9*B*).

RBCs from Individuals with Diabetes Show Increased Resistance to PLY and PFO—The significant positive correlation between Hba1c levels and PLY resistance of RBCs from individuals with diabetes not on metformin therapy motivated us to compare the susceptibility of RBCs from healthy and diabetic individuals to two members of the CDC family of PFTs, PLY and PFO. Fresh RBCs from healthy individuals ($n = 17$) and individuals with diabetes not on metformin therapy ($n = 13$) were incubated with purified recombinant PLY (118 ng/ml) or PFO (72 ng/ml), and cell lysis was monitored by phase contrast microscopy. Fig. 10 shows the average (± S.E.) hemolysis time profiles of the cells treated with the toxins. RBCs from diabetic individuals showed increased resistance to both PLY (Fig. 10*A*) and PFO (Fig. 10*B*), indicated by a right-shift of the hemolysis time profiles relative to healthy RBCs. At the toxin concentrations used, the time required to lyse 50% of the RBCs from individuals with diabetes has increased by ~6 min (on average) relative to control, healthy cells.

Diabetic RBCs Exhibit Increased Membrane Stiffness—In a separate set of experiments, we sought to establish whether the mechanical properties of the RBC plasma membrane are altered in diabetes. Using the micropipette aspiration method, we measured the modulus of shear elasticity of RBCs derived from diabetic subjects ($n = 12$) neither on insulin nor metformin treatment compared with healthy age-matched controls ($n = 14$). A summary of the measurements is shown in Fig. 11, from which the modulus of shear elasticity was evaluated. The average shear modulus for the controls was 5 ± 1 micronewtons/m, although for the diabetic group the average value was significantly higher, 12 ± 2 micronewtons/m.

Discussion

Membrane Biophysical Properties and Cell Susceptibility to PLY—The results obtained in this study paint a complex landscape of biophysical factors affecting the interaction between PLY and RBCs. Single cell studies carried out to assess the effect of the physical properties of the membrane on cell susceptibility

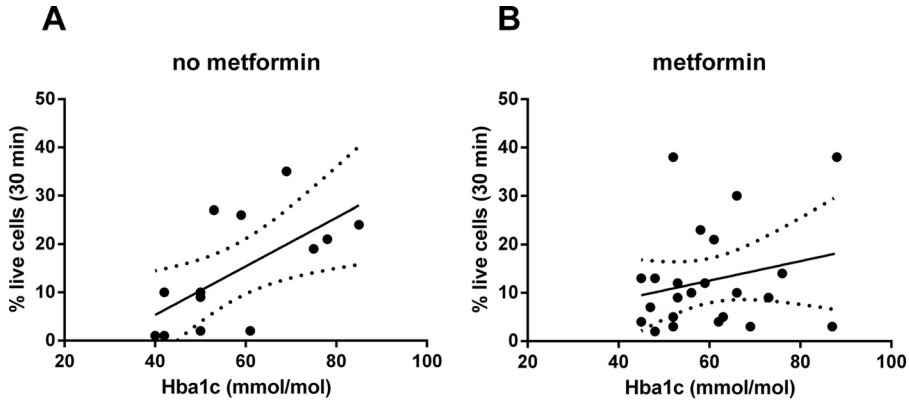

FIGURE 9. **Correlation between levels of Hba1c and susceptibility of RBCs from individuals with diabetes to PLY.** *A,* samples ($n = 13$) derived from subjects with diabetes not on metformin therapy: $R^2 = 0.410$, $p = 0.018$ (*). *B,* samples ($n = 23$) derived from subjects with diabetes on metformin therapy: $R^2 = 0.054$, $p = 0.285$ (not significant). RBCs from individuals with diabetes were exposed to PLY (118 ng/ml), and the percentage of live cells after exposure to toxin for 30 min was plotted against levels of Hba1c.

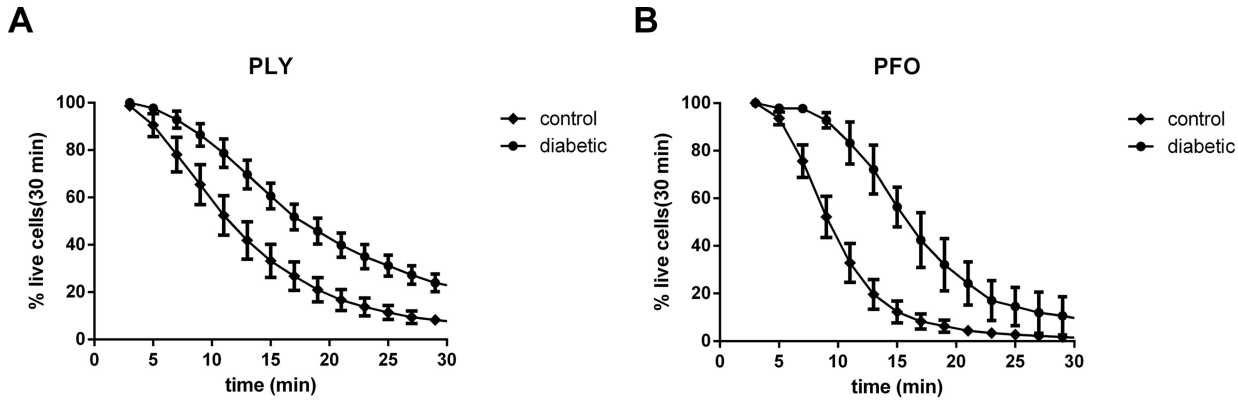

FIGURE 10. **RBCs from individuals with diabetes show increased resistance to PLY (*A*) and PFO (*B*) relative to RBCs from healthy control individuals.** Average (± S.E.) time course of hemolysis induced by PLY (118 ng/ml) or PFO (72 ng/ml) in RBCs from healthy individuals ($n = 17$) and individuals with diabetes not on metformin therapy ($n = 13$). Cell lysis was monitored by phase contrast microscopy for 30 min.

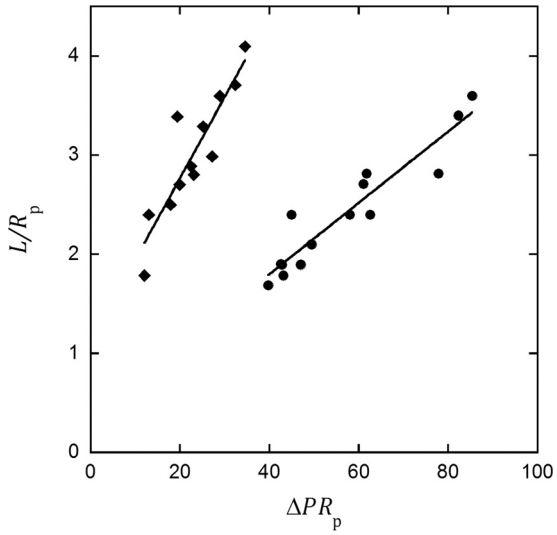

FIGURE 11. **Dependence of the measured projection length (*L*) on the applied pressure, Δ*P* (*L* and Δ*P* are scaled according to Equation 2), for samples derived from subjects with diabetes (●) and from healthy controls (◆).** Each point represents an average measurement for each group ($n = 12$ in the diabetic group and $n = 14$ in the healthy control group). The modulus of shear elasticity was evaluated from the gradient of the linear fits.

to toxin (Fig. 8) revealed that membrane elasticity and electrical properties in healthy RBCs are correlated with their susceptibility to PLY-induced lysis.

Surface charge density (and therefore surface potential) will modify the interactions of the membrane with charged molecules. Although the detailed charge distribution on the surface of a PLY monomer is complex (Fig. 12), the overall charge of the molecule is −15 (78). This, to the lowest approximation, would explain the observed dependence in Fig. 8*C*, which suggests that cells that naturally possess lower (negative) surface potential are more prone to hemolysis, probably due to the reduced electrostatic repulsion between the molecule of PLY and the RBC membrane. The reason for the marked electronegative potential of PLY in contrast to other CDCs is unclear (33).

The membrane dipole potential has its origins in the alignment of the lipid molecules (containing a number of dipoles mainly in the headgroup region) in the plane of the membrane and the orientation of water molecules in the immediate vicinity of the lipid headgroups (79–81). This potential has been reported to affect protein function (59), as well as insertion and secondary structure formation of peptides (76). Here, we have shown that healthy RBCs naturally characterized by higher magnitudes of the membrane dipole potential are more susceptible to PLY (Fig. 8*B*) and to the related toxin PFO (data not shown), probably due to increased cholesterol levels in these cells (see below) (59). In a similar trend, cells that exhibit higher bending rigidity of their membranes are easier to lyse by PLY. However, we must emphasize that these two parameters are not

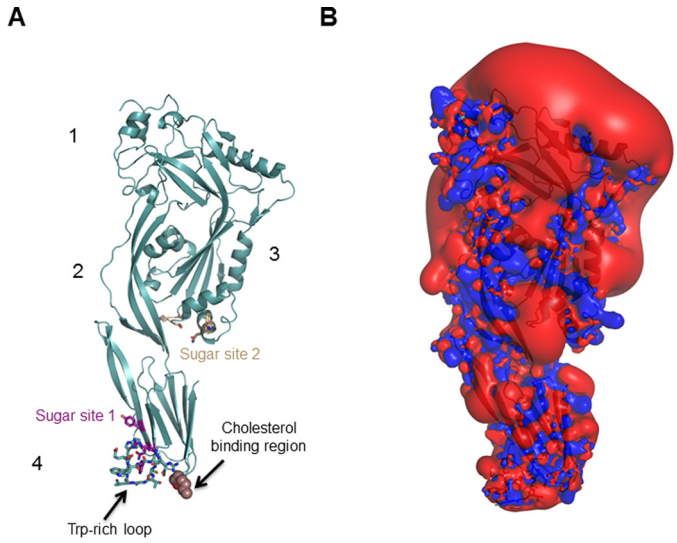

FIGURE 12. **Isosurface of PLY monomer.** *A, ribbon* representation of the PLY peptide backbone with the four domains numbered. The highly conserved tryptophan-rich loop and the cholesterol binding region at the base of domain 4 are shown in *stick and ball* representations, respectively. The two putative sugar-binding sites, site 1 near the conserved tryptophan-rich loop (*purple*) and site 2 at the domain 3-domain 4 interface (*gray*), are shown in *stick* representation. *B,* corresponding PLY isosurface was drawn at −1 (*red*) and +1 (*blue*) contour levels as calculated and drawn using the APBS (125, 126) add-on to PyMOL (127). The field projecting from the PLY monomer is mostly, but not completely, negative.

the sole and direct determinants of lytic resistance *per se*. This can be seen in comparison with cells pretreated with cumOOH (Fig. 5). We have previously shown that treatment of RBCs with cumOOH increased both the membrane bending elastic modulus (64) and membrane dipole potential (77), yet these cells are much more resistant to toxin compared with healthy cells, for which higher bending rigidity and dipole potential meant lower resistance to PLY (Fig. 8, *A* and *B*, respectively). Therefore, the origins of the correlations between these two properties and susceptibility to PLY in healthy cells should be sought in a common underpinning factor, such as the variations in molecular composition and supramolecular organization of the lipid membrane, which may alter the cell resistance to toxin, as well as the membrane physical properties.

Factors Affecting Cell Susceptibility to PLY—One of the likely factors suggested by the cell membrane modification studies (see below) is the age of the individual cells within the population. As a measure of the time spent by the cell in an environment characterized by chemical stresses, cell age is likely to alter the membrane physical properties. Indeed, a number of studies reported that RBC *deformability* decreases with cell age (for a comprehensive summary see Ref. 82). However, many of these measurements are method-dependent, and the reported quantities are often ambiguously defined. In addition, changes in the overall cell deformability are generally related to changes in viscosity of the cytoplasm, membrane fluidity, and membrane elasticity (82), which is further characterized by bending, shear, and area deformations (7). The two parameters we measure in this work, membrane bending modulus and dipole potential, reflect primarily the properties of the lipid bilayer, but to the best of our knowledge there are no comprehensive studies as to how these two properties would change with cell age. As a first approximation to the process of aging, we measured the bending elastic modulus of cells treated with DHEA but found no significant alterations from untreated cells (data not shown). DHEA inhibits glucose-6-phosphate dehydrogenase activity, and there are contradictory reports on RBC deformability in glucose-6-phosphate dehydrogenase-deficient subjects (83–85), but again, the methods used to assess cell deformability did not necessarily mean measuring the membrane bending elastic modulus. A detailed study of the effect of aging on RBC membrane physical properties (bending, shear, area elastic moduli, and membrane electrostatic potentials) falls beyond the scope of this study. Even though the membrane modification studies suggest that cell aging is a factor determining cell susceptibility to toxin, it would be too speculative to also attribute the correlations we established in Fig. 8, *A* and *B,* solely and exclusively to RBC age. It is also notable that we found no significant correlation between the age of the healthy donors (a parameter different from individual cell age in the same population) and the susceptibility of their RBCs to PLY (data not shown). Other factors are bound to play a significant role.

One of these factors is likely to be the membrane cholesterol content. It has been established that the presence of membrane cholesterol is an essential condition for successful insertion of PLY into membranes (1) and depletion of membrane cholesterol impairs the hemolytic activity of PLY (52). Natural variation in cholesterol content between different cells could then be responsible for the different binding of PLY to RBCs (Fig. 3); our measurements of membrane bending modulus (Fig. 8*A*) and membrane dipole potential (Fig. 8*B*) point in the same direction. It is well known that inclusion of cholesterol in bilayer membranes of lipids with either two saturated chains or one saturated and one monounsaturated chain leads to an increase of their bending elastic modulus (86–90). In membranes, cholesterol intercalates between lipid chains to form a highly ordered but laterally mobile liquid ordered phase, which is believed to be the basis of the membrane lipid rafts (91). This liquid ordered phase is characterized with higher magnitudes of its membrane dipole potential (59, 92). Thus, the fact that stiffer membranes and membranes with higher dipole potential are more susceptible to lysis is likely to reflect higher cholesterol content.

Although it is recognized that CDC binding to the lipid membrane requires the presence of cholesterol, it is also clear that its role in this process is complicated (93, 94), with significant differences (both quantitative and qualitative) between different CDC toxins. For example, studies using PFO revealed that membrane binding depends on the availability of "free cholesterol" at the membrane surface and does not correlate with the presence of detergent-resistant domains (93). In contrast, PLY has been reported to bind to cholesterol-rich lipid raft microdomains in corneal epithelial cells (95). Such differences suggest that the composition and organization (and hence physical properties) of the lipid bilayer itself is likely to be a key regulator of the interaction of CDCs with the membrane.

We also found that cell morphology has an effect on membrane susceptibility to PLY, with discocytes being more resistant than stomatocytes (Fig. 4). Interestingly, in a previous study

investigating the dependence of the membrane dipole potential in RBCs and ghosts on membrane curvature (77), we found that stomatocytes are characterized with higher membrane dipole potentials compared with discocytes, which could also have an effect on PLY recruitment to the membrane (*cf.* Fig. 8*B*). Additional imaging experiments with echinocytes revealed that toxin distribution along the surface of the echinocytic cells was non-uniform, with the majority of toxin clustering onto the highly curved membrane projections (Fig. 4*C*). These observations suggest that PLY may have curvature preference when binding to or diffusing along the membrane. Further studies would be necessary to clarify whether PLY has an intrinsic curvature preference or the effect is caused by curvature-driven sorting of lipids in the plasma membrane (96). If this is the case, such spatially restricted distribution may serve to effectively increase the local toxin concentration, leading to shorter diffusion distances and faster formation of oligomers, hence shorter lysis times.

Membrane Modification and Cell Susceptibility to PLY—It has previously been shown that reduction of extracellular calcium strongly enhances the lytic capacity of PLY due to increased membrane binding (97). One of the main findings of this study suggests that cell susceptibility to PLY also critically depends on the oxidative and/or other chemical stress the membrane has been subjected to before interaction with the toxin (Fig. 5). In addition, it demonstrates the non-universality of the effect of different oxidative agents, because the outcome, in terms of cell resistance to toxin, critically depends on the mode of action of each oxidant. This is evident by comparing the effects of the two oxidative agents used, H_2O_2 and cumOOH. H_2O_2 is water-soluble and readily partitions in the cytoplasm once it has crossed the lipid bilayer, where its primary target is hemoglobin. Oxidation and denaturing of hemoglobin leads to the formation of spectrin-globin complexes, changes spectrin network organization, and also causes clustering of the transmembrane protein band 3 (64, 98–101). Although H_2O_2 may affect the molecular organization in the lipid bilayer (99), the transbilayer lipid distribution is not affected, and its overall effect on the lipid bilayer is limited (64, 77, 99), hence the lack of effect on the susceptibility of RBCs to PLY. In contrast, direct oxidation of the lipid bilayer membrane with the membrane-bound cumOOH drastically affects the PLY-RBC interactions and makes the membrane much more resistant to toxin. This could be due to the chemical modification of PLY receptors on the membrane surface (40) and/or oxidation of cholesterol that could modulate the conformation of glycans necessary for the successful binding of the toxin to the RBC membrane (102). Direct cholesterol oxidation (103) will also affect the lateral microdomain organization of the lipid membrane (104–106), which could impair membrane insertion of the toxin, because PLY has been reported to bind to cholesterol-rich lipid raft microdomains (95). As a result, the membrane is rendered more impervious to toxin. Lipid oxidation also has an effect on the physical state of the membrane. We have previously shown that cumOOH leads to tighter in-plane lipid packing as demonstrated by an increase in the membrane dipole potential (77), as well as increased membrane bending and shear rigidity (64) (for a discussion of the membrane physical properties see above). Such changes in lipid packing may result in reduced ability of the toxin to insert into the plasma membrane.

In contrast to the effect of cumOOH, aging cells artificially using DHEA leads to lower resistance to PLY. DHEA inhibits glucose-6-phosphate dehydrogenase activity, which results in reduced levels of NADPH, an essential molecule in the cell's antioxidant defense system. Therefore, these cells are characterized with higher exposure to oxidative stress (presumably under conditions more similar to those *in vivo*), yet their response to PLY differs from both H_2O_2- and cumOOH-treated cells. This, once again, demonstrates that the general term "oxidative stress" is insufficient in describing the effect of oxidative agents on membrane response to toxin and that the mechanism of action of each oxidant should be considered on a case-by-case basis.

The final membrane modification we investigated, lipid scrambling caused by calcium ionophore A23187, led to increased cell resistance to PLY that correlates with impaired toxin binding. We designed this experiment to mimic aspects of eryptosis (the analogue of apoptosis in nucleated cells), which is characterized, among other processes, by lipid scrambling and exposure of PS on the outer leaflet of the lipid bilayer (58). Our results show that lipid scrambling is a factor for increased cell resistance to not only PLY (Fig. 5) but also to the related toxin PFO (data not shown), which suggests that cells set on the path of programmed death are also less likely to hemolyze under the lytic action of the toxin. This could be understood in terms of the asymmetry of the RBC lipid bilayer membrane. In human RBCs lipid species, such as PS and phosphatidylethanolamine, are much more abundant in the inner cytoplasmic leaflet, whereas phosphatidylcholine and sphingomyelin are found in larger concentrations in the outer leaflet (107). Scrambling of lipids would change the lipid composition in the leaflets as well as their lateral lipid organization. This will ultimately affect the interaction between the toxin and the membrane (see Fig. 7), because the toxin is expected to be attuned to effective interactions with the outer surface of the cell membrane, with which it establishes the first contact.

These observations led to the conclusion that at least one of the factors for the variability in the response of cells within the same population to toxin is likely to be the chemical and/or oxidative prehistory of each individual cell, which would be determined by the cell age in the circulation and the relevant health status of the individual. Cell modifications as a result of disease (*e.g.* conditions characterized by high levels of oxidative stress, such as diabetes (108)) may lead to altered susceptibility to virulence factors, consistent with our findings that RBCs from individuals with diabetes show increased resistance to PLY and PFO relative to healthy RBCs (Fig. 10). Susceptibility to CDCs may also be altered in diseases that affect the RBC cholesterol content, such as acute coronary syndrome where the cholesterol content of the erythrocyte membranes is increased (109) or in diseases that are characterized by PS externalization, such as sickle cell anemia (110), sepsis (111), and systemic sclerosis (112).

Susceptibility of RBCs from Individuals with Diabetes to PLY—Our cell modification studies provide a framework for understanding the diversity of response to PLY in RBCs from individuals with diabetes. We found that RBCs from individuals with higher levels of Hba1c, which presumably have been subjected to higher glucose concentrations or resided in the hyperglycemic milieu for longer periods of time, were more resistant to the toxin's lytic action (Figs. 9 and 10*A*). Increased resistance to PLY in RBCs from individuals with diabetes and higher levels of Hba1c could be understood in terms of elevated oxidative stress, to which the cell membrane is exposed in diabetes, and its consequent biochemical and biophysical modifications. Numerous studies have demonstrated that oxidative stress levels are higher in diabetes, and this plays an important role in the progression of the disease and its complications (113, 114). This is a consequence of the elevated glucose levels, leading to abundance of free radicals generated through glucose oxidation as well as non-enzymatic glycation of proteins and their subsequent oxidation (114). As discussed above, higher levels of oxidative stress would cause modification of the bilayer lipid membrane (including lipids, cholesterol, and membrane proteins) and/or PLY receptors on the surface, which in some cases may lead to increased resistance to PLY (*cf.* Fig. 5). In this context, Hba1c can be considered as a measure of the oxidative stress levels, to which the cells have been exposed. Further evidence for the altered RBC membrane physical properties in diabetes is presented in Fig. 11, showing that for diabetic cells the membrane shear elastic modulus is more than twice the value of age-matched controls. Such stiffening of the membrane is suggestive of the involvement of oxidative processes, as demonstrated previously (64, 99, 115), and supports our conclusion that increased hemolytic resistance of RBCs from diabetic individuals is due to oxidative modifications of their membranes.

To the extent that the RBC membrane is representative of plasma membranes of other cell types, our studies on RBCs from individuals with diabetes suggest that the increased association of *S. pneumoniae* with disease in individuals with diabetes may not necessarily be related to the direct and immediate hemolytic action of PLY. It is known that diabetic patients often have impaired immune functions (116), and this may outweigh the increased resistance of cells to the action of the toxin, providing other routes through which the adverse effects of *S. pneumoniae* could occur. Alternatively, the reduced hemolytic activity of PLY in individuals with diabetes may favor the initial survival and proliferation of *S. pneumoniae* in the blood. Such an interpretation is supported by a recent study showing that PLY with low hemolytic activity conferred an early growth advantage to *S. pneumoniae* in the blood compared with strains expressing PLY with full hemolytic activity (117). PLY also has non-cytolytic, complement-activating properties that act independently of its cytolytic activity (118, 119).

It is important to note the differences between the two subsets of diabetic individuals investigated in this study (Fig. 9, *A* and *B*). The dependence of the susceptibility of RBCs to PLY on Hba1c appears to be much weaker in individuals treated with metformin (to the point of being statistically insignificant). Metformin is a common anti-hyperglycemic agent for the treatment of type 2 diabetes, and it is thought to help prevent complications by increasing cell sensitivity to insulin (120), thereby providing satisfactory glucose control. However, there is evidence that metformin may offer further benefits by reducing the levels of glyoxal and methylglyoxal and preventing the formation of advanced glycation end products (121, 122). Recent studies have also suggested that metformin could reduce the production of reactive oxidative species (120, 123). Our previous *in vitro* experiments on RBC membrane elasticity demonstrated that, although glycated RBCs are more susceptible to oxidative stress than normal cells, the metformin is able to ameliorate considerably the increased vulnerability of glycated cells to oxidative stress (124). These results suggest that oxidation-induced membrane modifications may be significantly reduced in the presence of metformin, and this could be the main factor explaining the difference in the response of diabetic cells to toxin between the two groups (Fig. 9, *A* and *B*).

Conclusion—In conclusion, our studies indicate that the diversity of response to PLY within a population of RBCs is influenced by the biophysical, biochemical, and morphological properties of the plasma membrane and is also correlated to membrane modifications in diabetes. These results are not only relevant to understanding the interactions between pore-forming toxins and RBCs but also (to the extent that the RBC membrane serves as a model of eukaryotic cell membranes) to understanding the behavior of toxins in tissues. We believe that our findings are relevant to other CDCs, and similar methodology can readily be employed for assessing cell susceptibility to a variety of other pore-forming toxins.

Author Contributions—M. B. B. conducted most of the experiments, analyzed the results, and wrote the paper with P. G. P. P. G. P. designed research, analyzed parts of the results, and wrote the paper with M. B. B. M. A. K. carried out the micropipette experiments. C. P. W. and R. W. T. conceived the idea for the project, coordinated the study, and revised the manuscript. C. E. N. prepared Fig. 12 and assisted in the preparation of the manuscript. M. K. M. generated, expressed, and purified PLY and most of its derivatives. T. J. M. assisted in the preparation of the manuscript and revised the manuscript. A. C. S., K. M. G., and F. C. made contributions to the design of the research, recruited participants, and acquired samples and data. All authors reviewed the results and approved the final version of the manuscript.

Acknowledgments—We thank E. Green, S. A. Jewell, P. Gologan, M. J. Smallwood, and R. Tennant for their help with the experimental techniques. We also thank the NIHR Exeter Clinical Research Facility for making red blood cells available.

References

1. Giddings, K. S., Johnson, A. E., and Tweten, R. K. (2003) Redefining cholesterol's role in the mechanism of the cholesterol-dependent cytolysins. *Proc. Natl. Acad. Sci. U.S.A.* **100,** 11315–11320
2. Deuticke, B. (2003) in *Red Cell Membrane Transport in Health and Disease* (Bernhardt, I., and Ellory, J. C., eds) pp. 27–60, Springer, Berlin
3. Hess, J. R., Sparrow, R. L., van der Meer, P. F., Acker, J. P., Cardigan, R. A., and Devine, D. V. (2009) Red blood cell hemolysis during blood bank storage: using national quality management data to answer basic scientific questions. *Transfusion* **49,** 2599–2603
4. Waugh, R. E., Narla, M., Jackson, C. W., Mueller, T. J., Suzuki, T., and Dale, G. L. (1992) Rheologic properties of senescent erythrocytes: loss of

surface area and volume with red blood cell age. *Blood* **79,** 1351–1358
5. Tomaiuolo, G., Rossi, D., Caserta, S., Cesarelli, M., and Guido, S. (2012) Comparison of two flow-based imaging methods to measure individual red blood cell area and volume. *Cytometry A* **81,** 1040–1047
6. Mokken, F. C., Kedaria, M., Henny, C. P., Hardeman, M. R., and Gelb, A. W. (1992) The clinical importance of erythrocyte deformability, a hemorrheological parameter. *Ann. Hematol.* **64,** 113–122
7. Lim, H. W., G., Wortis, M., and Mukhopadhyay, R. (2008) *Red Blood Cell Shapes and Shape Transformations: Newtonian Mechanics of a Composite Membrane: Lipid Bilayers and Red Blood Cells* (Gompper, G., and Schick, M., eds) Vol. 4, Sections 2.1–2.4, Wiley-VCH Verlag GmbH & Co. KGaA, Weinheim, Germany, 10.1002/9783527623372.ch2a
8. Ciccoli, L., De Felice, C., Paccagnini, E., Leoncini, S., Pecorelli, A., Signorini, C., Belmonte, G., Guerranti, R., Cortelazzo, A., Gentile, M., Zollo, G., Durand, T., Valacchi, G., Rossi, M., and Hayek, J. (2013) Erythrocyte shape abnormalities, membrane oxidative damage, and β-actin alterations: an unrecognized triad in classical autism. *Mediators Inflamm.* **2013,** 432616
9. Cluitmans, J. C., Chokkalingam, V., Janssen, A. M., Brock, R., Huck, W. T., and Bosman, G. J. (2014) Alterations in red blood cell deformability during storage: a microfluidic approach. *Biomed. Res. Int.* **2014,** 764268
10. Pretorius, E., Swanepoel, A. C., Buys, A. V., Vermeulen, N., Duim, W., and Kell, D. B. (2014) Eryptosis as a marker of Parkinson's disease. *Aging* **6,** 788–819
11. Buys, A. V., Van Rooy, M. J., Soma, P., Van Papendorp, D., Lipinski, B., and Pretorius, E. (2013) Changes in red blood cell membrane structure in type 2 diabetes: a scanning electron and atomic force microscopy study. *Cardiovasc. Diabetol.* **12,** 25
12. Little, C., and Rumsby, M. G. (1980) Lysis of erythrocytes from stored human blood by phospholipase C (*Bacillus cereus*). *Biochem. J.* **188,** 39–46
13. Turchetti, V., De Matteis, C., Leoncini, F., Trabalzini, L., Guerrini, M., and Forconi, S. (1997) Variations of erythrocyte morphology in different pathologies. *Clin. Hemorheol. Microcirc.* **17,** 209–215
14. Siegl, C., Hamminger, P., Jank, H., Ahting, U., Bader, B., Danek, A., Gregory, A., Hartig, M., Hayflick, S., Hermann, A., Prokisch, H., Sammler, E. M., Yapici, Z., Prohaska, R., and Salzer, U. (2013) Alterations of red cell membrane properties in neuroacanthocytosis. *PLoS ONE* **8,** e76715
15. Tziakas, D., Chalikias, G., Grapsa, A., Gioka, T., Tentes, I., and Konstantinides, S. (2012) Red blood cell distribution width: a strong prognostic marker in cardiovascular disease: is associated with cholesterol content of erythrocyte membrane. *Clin. Hemorheol. Microcirc.* **51,** 243–254
16. Evans, T. C., and Jehle, D. (1991) The red blood cell distribution width. *J. Emerg. Med.* **9,** 71–74
17. Montagnana, M., Cervellin, G., Meschi, T., and Lippi, G. (2012) The role of red blood cell distribution width in cardiovascular and thrombotic disorders. *Clin. Chem. Lab. Med.* **50,** 635–641
18. Ye, Z., Smith, C., and Kullo, I. J. (2011) Usefulness of red cell distribution width to predict mortality in patients with peripheral artery disease. *Am. J. Cardiol.* **107,** 1241–1245
19. Gifford, S. C., Derganc, J., Shevkoplyas, S. S., Yoshida, T., and Bitensky, M. W. (2006) A detailed study of time-dependent changes in human red blood cells: from reticulocyte maturation to erythrocyte senescence. *Br. J. Haematol.* **135,** 395–404
20. Bratosin, D., Mazurier, J., Tissier, J. P., Estaquier, J., Huart, J. J., Ameisen, J. C., Aminoff, D., and Montreuil, J. (1998) Cellular and molecular mechanisms of senescent erythrocyte phagocytosis by macrophages. A review. *Biochimie* **80,** 173–195
21. Celedón, G., González, G., Barrientos, D., Pino, J., Venegas, F., Lissi, E. A., Soto, C., Martinez, D., Alvarez, C., and Lanio, M. E. (2008) Stycholysin II, a cytolysin from the sea anemone *Stichodactyla helianthus* promotes higher hemolysis in aged red blood cells. *Toxicon* **51,** 1383–1390
22. Shukla, S. D., Coleman, R., Finean, J. B., and Michell, R. H. (1978) The use of phospholipase c to detect structural changes in the membranes of human erythrocytes aged by storage. *Biochim. Biophys. Acta* **512,** 341–349
23. Saito, M., Ando, S., Tanaka, Y., Nagai, Y., Mitsui, K., and Hase, J. (1982) Age-development changes in susceptibility of erythrocytes to perfringolysin O. *Mech. Ageing Dev.* **20,** 53–63
24. Kantor, L., and Fackrell, H. B. (1994) Differential action of staphylococcal α-toxin on young and old erythrocytes. *Gerontology* **40,** 1–7
25. Kantor, L., and Fackrell, H. B. (1998) Senescent erythrocytes exhibit a single-hit response to staphylococcal α toxin. *Gerontology* **44,** 26–31
26. O'Callaghan, R. J., McCormick, C. C., Caballero, A. R., Marquart, M. E., Gatlin, H. P., and Fratkin, J. D. (2007) Age-related differences in rabbits during experimental *Staphylococcus aureus* keratitis. *Invest. Ophthalmol. Vis. Sci.* **48,** 5125–5131
27. Arese, P., Turrini, F., and Schwarzer, E. (2005) Band 3/complement-mediated recognition and removal of normally senescent and pathological human erythrocytes. *Cell. Physiol. Biochem.* **16,** 133–146
28. Fortin, C. F., Larbi, A., Lesur, O., Douziech, N., and Fulop, T., Jr. (2006) Impairment of SHP-1 down-regulation in the lipid rafts of human neutrophils under GM-CSF stimulation contributes to their age-related, altered functions. *J. Leukocyte Biol.* **79,** 1061–1072
29. Tweten, R. K., Parker, M. W., and Johnson, A. E. (2001) The cholesterol-dependent cytolysins. *Curr. Top. Microbiol. Immunol.* **257,** 15–33
30. Feldman, C., and Anderson, R. (2014) Recent advances in our understanding of *Streptococcus pneumoniae* infection. *F1000Prime Rep.* **6,** 82
31. Mitchell, T. J., and Dalziel, C. E. (2014) in *MACPF/CDC Proteins–Agents of Defence, Attack and Invasion* (Anderluh, G. and Gilbert, R., eds) pp. 145–160, Springer, Netherlands
32. Ortqvist, A., Hedlund, J., and Kalin, M. (2005) *Streptococcus pneumoniae*: epidemiology, risk factors, and clinical features. *Semin. Respir. Crit. Care Med.* **26,** 563–574
33. Lawrence, S. L., Feil, S. C., Morton, C. J., Farrand, A. J., Mulhern, T. D., Gorman, M. A., Wade, K. R., Tweten, R. K., and Parker, M. W. (2015) Crystal structure of *Streptococcus pneumoniae* pneumolysin provides key insights into early steps of pore formation. *Sci. Rep.* **5,** 14352
34. Marshall, J. E., Faraj, B. H., Gingras, A. R., Lonnen, R., Sheikh, M. A., El-Mezgueldi, M., Moody, P. C., Andrew, P. W., and Wallis, R. (2015) The crystal structure of pneumolysin at 2.0 A resolution reveals the molecular packing of the pre-pore complex. *Sci. Rep.* **5,** 13293
35. Soltani, C. E., Hotze, E. M., Johnson, A. E., and Tweten, R. K. (2007) Structural elements of the cholesterol-dependent cytolysins that are responsible for their cholesterol-sensitive membrane interactions. *Proc. Natl. Acad. Sci. U.S.A.* **104,** 20226–20231
36. Ramachandran, R., Heuck, A. P., Tweten, R. K., and Johnson, A. E. (2002) Structural insights into the membrane-anchoring mechanism of a cholesterol-dependent cytolysin. *Nat. Struct. Biol.* **9,** 823–827
37. Farrand, A. J., LaChapelle, S., Hotze, E. M., Johnson, A. E., and Tweten, R. K. (2010) Only two amino acids are essential for cytolytic toxin recognition of cholesterol at the membrane surface. *Proc. Natl. Acad. Sci. U.S.A.* **107,** 4341–4346
38. Shimada, Y., Maruya, M., Iwashita, S., and Ohno-Iwashita, Y. (2002) The C-terminal domain of perfringolysin O is an essential cholesterol-binding unit targeting to cholesterol-rich microdomains. *Eur. J. Biochem.* **269,** 6195–6203
39. Waheed, A. A., Shimada, Y., Heijnen, H. F., Nakamura, M., Inomata, M., Hayashi, M., Iwashita, S., Slot, J. W., and Ohno-Iwashita, Y. (2001) Selective binding of perfringolysin O derivative to cholesterol-rich membrane microdomains (rafts). *Proc. Natl. Acad. Sci. U.S.A.* **98,** 4926–4931
40. Shewell, L. K., Harvey, R. M., Higgins, M. A., Day, C. J., Hartley-Tassell, L. E., Chen, A. Y., Gillen, C. M., James, D. B., Alonzo, F., 3rd, Torres, V. J., Walker, M. J., Paton, A. W., Paton, J. C., and Jennings, M. P. (2014) The cholesterol-dependent cytolysins pneumolysin and streptolysin O require binding to red blood cell glycans for hemolytic activity. *Proc. Natl. Acad. Sci. U.S.A.* **111,** E5312–E5320
41. Ramachandran, R., Tweten, R. K., and Johnson, A. E. (2004) Membrane-dependent conformational changes initiate cholesterol-dependent cytolysin oligomerization and intersubunit β-strand alignment. *Nat. Struct. Mol. Biol.* **11,** 697–705
42. Tweten, R. K. (2005) Cholesterol-dependent cytolysins, a family of versatile pore-forming toxins. *Infect. Immun.* **73,** 6199–6209
43. Shatursky, O., Heuck, A. P., Shepard, L. A., Rossjohn, J., Parker, M. W., Johnson, A. E., and Tweten, R. K. (1999) The mechanism of membrane

insertion for a cholesterol-dependent cytolysin: a novel paradigm for pore-forming toxins. *Cell* **99,** 293–299
44. Tilley, S. J., Orlova, E. V., Gilbert, R. J., Andrew, P. W., and Saibil, H. R. (2005) Structural basis of pore formation by the bacterial toxin pneumolysin. *Cell* **121,** 247–256
45. Wade, K. R., Hotze, E. M., Kuiper, M. J., Morton, C. J., Parker, M. W., and Tweten, R. K. (2015) An intermolecular electrostatic interaction controls the prepore-to-pore transition in a cholesterol-dependent cytolysin. *Proc. Natl. Acad. Sci. U.S.A.* **112,** 2204–2209
46. Watanabe, I., Nomura, T., Tominaga, T., Yamamoto, K., Kohda, C., Kawamura, I., and Mitsuyama, M. (2006) Dependence of the lethal effect of pore-forming haemolysins of Gram-positive bacteria on cytolytic activity. *J. Med. Microbiol.* **55,** 505–510
47. Kadioglu, A., Weiser, J. N., Paton, J. C., and Andrew, P. W. (2008) The role of *Streptococcus pneumoniae* virulence factors in host respiratory colonization and disease. *Nat. Rev. Microbiol.* **6,** 288–301
48. Kirkham, L. A., Kerr, A. R., Douce, G. R., Paterson, G. K., Dilts, D. A., Liu, D. F., and Mitchell, T. J. (2006) Construction and immunological characterization of a novel nontoxic protective pneumolysin mutant for use in future pneumococcal vaccines. *Infect. Immun.* **74,** 586–593
49. Mughal, M. K. (2014) *Development of Pneumolysin as a Vaccine Candidate.* Ph.D. thesis, University of Glasgow, Glasgow, Scotland, United Kingdom
50. Solovyova, A. S., Nöllmann, M., Mitchell, T. J., and Byron, O. (2004) The solution structure and oligomerization behavior of two bacterial toxins: pneumolysin and perfringolysin O. *Biophys. J.* **87,** 540–552
51. Bokori-Brown, M., Kokkinidou, M. C., Savva, C. G., Fernandes da Costa, S., Naylor, C. E., Cole, A. R., Moss, D. S., Basak, A. K., and Titball, R. W. (2013) *Clostridium perfringens* **ϵ**-toxin H149A mutant as a platform for receptor binding studies. *Protein Sci.* **22,** 650–659
52. Lim, J. E., Park, S. A., Bong, S. M., Chi, Y. M., and Lee, K. S. (2013) Characterization of pneumolysin from *Streptococcus pneumoniae*, interacting with carbohydrate moiety and cholesterol as a component of cell membrane. *Biochem. Biophys. Res. Commun.* **430,** 659–663
53. Rasband, W. S. (2015) ImageJ, U. S. National Institutes of Health, Bethesda, MD, http://imagej.nih.gov/ij/
54. Hamilton, N. M., Dawson, M., Fairweather, E. E., Hamilton, N. S., Hitchin, J. R., James, D. I., Jones, S. D., Jordan, A. M., Lyons, A. J., Small, H. F., Thomson, G. J., Waddell, I. D., and Ogilvie, D. J. (2012) Novel steroid inhibitors of glucose-6-phosphate dehydrogenase. *J. Med. Chem.* **55,** 4431–4445
55. Henseleit, U., Plasa, G., and Haest, C. (1990) Effects of divalent cations on lipid flip-flop in the human erythrocyte membrane. *Biochim. Biophys. Acta* **1029,** 127–135
56. de Jong, K., Geldwerth, D., and Kuypers, F. A. (1997) Oxidative damage does not alter membrane phospholipid asymmetry in human erythrocytes. *Biochemistry* **36,** 6768–6776
57. Lang, K. S., Duranton, C., Poehlmann, H., Myssina, S., Bauer, C., Lang, F., Wieder, T., and Huber, S. M. (2003) Cation channels trigger apoptotic death of erythrocytes. *Cell Death Differ.* **10,** 249–256
58. Föller, M., Huber, S. M., and Lang, F. (2008) Erythrocyte programmed cell death. *IUBMB Life* **60,** 661–668
59. Starke-Peterkovic, T., Turner, N., Vitha, M. F., Waller, M. P., Hibbs, D. E., and Clarke, R. J. (2006) Cholesterol effect on the dipole potential of lipid membranes. *Biophys. J.* **90,** 4060–4070
60. Wall, J., Golding, C. A., Van Veen, M., and O'Shea, P. (1995) The use of fluoresceinphosphatidylethanolamine (FPE) as a real-time probe for peptide-membrane interactions. *Mol. Membr. Biol.* **12,** 183–192
61. Fitchen, N., O'Shea, P., Williams, P., and Hardie, K. R. (2003) Electrostatic sensor for identifying interactions between peptides and bacterial membranes. *Mol. Immunol.* **40,** 407–411
62. Cladera, J., Martin, I., and O'Shea, P. (2001) The fusion domain of HIV gp41 interacts specifically with heparan sulfate on the T-lymphocyte cell surface. *EMBO J.* **20,** 19–26
63. Hale, J. P., Marcelli, G., Parker, K. H., Winlove, C. P., and Petrov, P. G. (2009) Red blood cell thermal fluctuations: comparison between experiment and molecular dynamics simulations. *Soft Matter* **5,** 3603–3606
64. Hale, J. P., Winlove, C. P., and Petrov, P. G. (2011) Effect of hydroperoxides on red blood cell membrane mechanical properties. *Biophys. J.* **101,** 1921–1929
65. Waugh, R., and Evans, E. A. (1979) Thermoelasticity of red blood cell membrane. *Biophys. J.* **26,** 115–131
66. Chien, S., Sung, K. L., Skalak, R., Usami, S., and Tözeren, A. (1978) Theoretical and experimental studies on viscoelastic properties of erythrocyte membrane. *Biophys. J.* **24,** 463–487
67. Soler-Jover, A., Blasi, J., Gómez de Aranda, I., Navarro, P., Gibert, M., Popoff, M. R., and Martín-Satué, M. (2004) Effect of **ϵ** toxin-GFP on MDCK cells and renal tubules *in vivo*. *J. Histochem. Cytochem.* **52,** 931–942
68. Yamaji-Hasegawa, A., Makino, A., Baba, T., Senoh, Y., Kimura-Suda, H., Sato, S. B., Terada, N., Ohno, S., Kiyokawa, E., Umeda, M., and Kobayashi, T. (2003) Oligomerization and pore formation of a sphingomyelin-specific toxin, lysenin. *J. Biol. Chem.* **278,** 22762–22770
69. Yilmaz, N., Yamada, T., Greimel, P., Uchihashi, T., Ando, T., and Kobayashi, T. (2013) Real-time visualization of assembling of a sphingomyelin-specific toxin on planar lipid membranes. *Biophys. J.* **105,** 1397–1405
70. van den Berg, J. J., Op den Kamp, J. A., Lubin, B. H., Roelofsen, B., and Kuypers, F. A. (1992) Kinetics and site specificity of hydroperoxide-induced oxidative damage in red blood cells. *Free Radic. Biol. Med.* **12,** 487–498
71. Mishra, R., Sarkar, D., Bhattacharya, S., Mallick, S., Chakraborty, M., Mukherjee, D., Kar, M., and Mishra, R. (2015) Quantifying morphological alteration of RBC population from light scattering data. *Clin. Hemorheol. Microcirc.* **59,** 287–300
72. Barrera, F. N., Fendos, J., and Engelman, D. M. (2012) Membrane physical properties influence transmembrane helix formation. *Proc. Natl. Acad. Sci. U.S.A.* **109,** 14422–14427
73. Harris, F. M., Smith, S. K., and Bell, J. D. (2001) Physical properties of erythrocyte ghosts that determine susceptibility to secretory phospholipase A_2. *J. Biol. Chem.* **276,** 22722–22731
74. Asawakarn, T., Cladera, J., and O'Shea, P. (2001) Effects of the membrane dipole potential on the interaction of saquinavir with phospholipid membranes and plasma membrane receptors of Caco-2 cells. *J. Biol. Chem.* **276,** 38457–38463
75. Evans, E., and Needham, D. (1987) Physical properties of surfactant bilayer membranes: thermal transitions, elasticity, rigidity, cohesion and colloidal interactions. *J. Phys. Chem.* **91,** 4219–4228
76. Cladera, J., and O'Shea, P. (1998) Intramembrane molecular dipoles affect the membrane insertion and folding of a model amphiphilic peptide. *Biophys. J.* **74,** 2434–2442
77. Jewell, S. A., Petrov, P. G., and Winlove, C. P. (2013) The effect of oxidative stress on the membrane dipole potential of human red blood cells. *Biochim. Biophys. Acta* **1828,** 1250–1258
78. Rossjohn, J., Gilbert, R. J., Crane, D., Morgan, P. J., Mitchell, T. J., Rowe, A. J., Andrew, P. W., Paton, J. C., Tweten, R. K., and Parker, M. W. (1998) The molecular mechanism of pneumolysin, a virulence factor from *Streptococcus pneumoniae*. *J. Mol. Biol.* **284,** 449–461
79. Bechinger, B., and Seelig, J. (1991) Interaction of electric dipoles with phospholipid head groups. A deuterium and phosphorus-31 NMR study of phloretin and phloretin analogs in phosphatidylcholine membranes. *Biochemistry* **30,** 3923–3929
80. Gawrisch, K., Ruston, D., Zimmerberg, J., Parsegian, V. A., Rand, R. P., and Fuller, N. (1992) Membrane dipole potentials, hydration forces, and the ordering of water at membrane surfaces. *Biophys. J.* **61,** 1213–1223
81. Brockman, H. (1994) Dipole potential of lipid membranes. *Chem. Phys. Lipids* **73,** 57–79
82. Shiga, T., Maeda, N., and Kon, K. (1990) Erythrocyte rheology. *Crit. Rev. Oncol. Hematol.* **10,** 9–48
83. Johnson, G. J., Allen, D. W., Cadman, S., Fairbanks, V. F., White, J. G., Lampkin, B. C., and Kaplan, M. E. (1979) Red-cell-membrane polypeptide aggregates in glucose-6-phosphate dehydrogenase mutants with chronic hemolytic disease: a clue to the mechanism of hemolysis. *N. Engl. J. Med.* **301,** 522–527
84. Johnson, R. M., Ravindranath, Y., ElAlfy, M. S., El-Alfy, M., and Goyette, G., Jr. (1994) Oxidant damage to erythrocyte membrane in glucose-6-

phosphate dehydrogenase deficiency: correlation with *in vivo* reduced glutathione concentration and membrane protein oxidation. *Blood* **83,** 1117–1123
85. Gurbuz, N., Yalcin, O., Aksu, T. A., and Baskurt, O. K. (2004) The relationship between the enzyme activity, lipid peroxidation and red blood cells deformability in hemizygous and heterozygous glucose-6-phosphate dehydrogenase deficient individuals. *Clin. Hemorheol. Microcirc.* **31,** 235–242
86. Evans, E., and Rawicz, W. (1990) Entropy-driven tension and bending elasticity in condensed-fluid membranes. *Phys. Rev. Lett.* **64,** 2094–2097
87. Song, J., and Waugh, R. E. (1993) Bending rigidity of SOPC membranes containing cholesterol. *Biophys. J.* **64,** 1967–1970
88. Méléard, P., Gerbeaud, C., Pott, T., Fernandez-Puente, L., Bivas, I., Mitov, M. D., Dufourcq, J., and Bothorel, P. (1997) Bending elasticities of model membranes: influences of temperature and sterol content. *Biophys. J.* **72,** 2616–2629
89. Henriksen, J., Rowat, A. C., and Ipsen, J. H. (2004) Vesicle fluctuation analysis of the effects of sterols on membrane bending rigidity. *Eur. Biophys. J.* **33,** 732–741
90. Pan, J., Mills, T. T., Tristram-Nagle, S., and Nagle, J. F. (2008) Cholesterol perturbs lipid bilayers nonuniversally. *Phys. Rev. Lett.* **100,** 198103
91. Ohvo-Rekilä, H., Ramstedt, B., Leppimäki, P., and Slotte, J. P. (2002) Cholesterol interactions with phospholipids in membranes. *Prog. Lipid Res.* **41,** 66–97
92. Duggan, J., Jamal, G., Tilley, M., Davis, B., McKenzie, G., Vere, K., Somekh, M. G., O'Shea, P., and Harris, H. (2008) Functional imaging of microdomains in cell membranes. *Eur. Biophys. J.* **37,** 1279–1289
93. Flanagan, J. J., Tweten, R. K., Johnson, A. E., and Heuck, A. P. (2009) Cholesterol exposure at the membrane surface is necessary and sufficient to trigger perfringolysin O binding. *Biochemistry* **48,** 3977–3987
94. Heuck, A. P., Hotze, E. M., Tweten, R. K., and Johnson, A. E. (2000) Mechanism of membrane insertion of a multimeric β-barrel protein: perfringolysin O creates a pore using ordered and coupled conformational changes. *Mol. Cell* **6,** 1233–1242
95. Taylor, S. D., Sanders, M. E., Tullos, N. A., Stray, S. J., Norcross, E. W., McDaniel, L. S., and Marquart, M. E. (2013) The cholesterol-dependent cytolysin pneumolysin from *Streptococcus pneumoniae* binds to lipid raft microdomains in human corneal epithelial cells. *PLoS ONE* **8,** e61300
96. Callan-Jones, A., Sorre, B., and Bassereau, P. (2011) Curvature-driven lipid sorting in biomembranes. *Cold Spring Harb. Perspect. Biol.* **3,** a004648
97. Wippel, C., Förtsch, C., Hupp, S., Maier, E., Benz, R., Ma, J., Mitchell, T. J., and Iliev, A. I. (2011) Extracellular calcium reduction strongly increases the lytic capacity of pneumolysin from *Streptococcus pneumoniae* in brain tissue. *J. Infect. Dis.* **204,** 930–936
98. Low, P. S., Waugh, S. M., Zinke, K., and Drenckhahn, D. (1985) The role of hemoglobin denaturation and band 3 clustering in red blood cell aging. *Science* **227,** 531–533
99. Snyder, L. M., Fortier, N. L., Trainor, J., Jacobs, J., Leb, L., Lubin, B., Chiu, D., Shohet, S., and Mohandas, N. (1985) Effect of hydrogen peroxide exposure on normal human erythrocyte deformability, morphology, surface characteristics, and spectrin-hemoglobin cross-linking. *J. Clin. Invest.* **76,** 1971–1977
100. Fortier, N., Snyder, L. M., Garver, F., Kiefer, C., McKenney, J., and Mohandas, N. (1988) The relationship between *in vivo* generated hemoglobin skeletal protein complex and increased red cell membrane rigidity. *Blood* **71,** 1427–1431
101. McPherson, R. A., Sawyer, W. H., and Tilley, L. (1992) Rotational diffusion of the erythrocyte integral membrane protein, band 3: effect of hemichrome binding. *Biochemistry* **31,** 512–518
102. Lingwood, D., Binnington, B., Róg, T., Vattulainen, I., Grzybek, M., Coskun, U., Lingwood, C. A., and Simons, K. (2011) Cholesterol modulates glycolipid conformation and receptor activity. *Nat. Chem. Biol.* **7,** 260–262
103. Niki, E., Yoshida, Y., Saito, Y., and Noguchi, N. (2005) Lipid peroxidation: mechanisms, inhibition, and biological effects. *Biochem. Biophys. Res. Commun.* **338,** 668–676
104. Rooney, M., Tamura-Lis, W., Lis, L. J., Yachnin, S., Kucuk, O., and Kauffman, J. W. (1986) The influence of oxygenated sterol compounds on dipalmitoylphosphatidylcholine bilayer structure and packing. *Chem. Phys. Lipids* **41,** 81–92
105. Massey, J. B., and Pownall, H. J. (2006) Structures of biologically active oxysterols determine their differential effects on phospholipid membranes. *Biochemistry* **45,** 10747–10758
106. Davis, S., Davis, B. M., Richens, J. L., Vere, K. A., Petrov, P. G., Winlove, C. P., and O'Shea, P. (2015) α-Tocopherols modify the membrane dipole potential leading to modulation of ligand binding by P-glycoprotein. *J. Lipid Res.* **56,** 1543–1550
107. Rothman, J. E., and Lenard, J. (1977) Membrane asymmetry. *Science* **195,** 743–753
108. Amer, J., Etzion, Z., Bookchin, R. M., and Fibach, E. (2006) Oxidative status of valinomycin-resistant normal, β-thalassemia and sickle red blood cells. *Biochim. Biophys. Acta* **1760,** 793–799
109. Tziakas, D. N., Kaski, J. C., Chalikias, G. K., Romero, C., Fredericks, S., Tentes, I. K., Kortsaris, A. X., Hatseras, D. I., and Holt, D. W. (2007) Total cholesterol content of erythrocyte membranes is increased in patients with acute coronary syndrome: a new marker of clinical instability? *J. Am. Coll. Cardiol.* **49,** 2081–2089
110. Yasin, Z., Witting, S., Palascak, M. B., Joiner, C. H., Rucknagel, D. L., and Franco, R. S. (2003) Phosphatidylserine externalization in sickle red blood cells: associations with cell age, density, and hemoglobin F. *Blood* **102,** 365–370
111. Kempe, D. S., Akel, A., Lang, P. A., Hermle, T., Biswas, R., Muresanu, J., Friedrich, B., Dreischer, P., Wolz, C., Schumacher, U., Peschel, A., Götz, F., Döring, G., Wieder, T., Gulbins, E., and Lang, F. (2007) Suicidal erythrocyte death in sepsis. *J. Mol. Med.* **85,** 273–281
112. Giovannetti, A., Gambardella, L., Pietraforte, D., Rosato, E., Giammarioli, A. M., Salsano, F., Malorni, W., and Straface, E. (2012) Red blood cell alterations in systemic sclerosis: a pilot study. *Cell. Physiol. Biochem.* **30,** 418–427
113. Kennedy, A. L., and Lyons, T. J. (1997) Glycation, oxidation, and lipoxidation in the development of diabetic complications. *Metabolism* **46,** 14–21
114. Maritim, A. C., Sanders, R. A., and Watkins, J. B., 3rd (2003) Diabetes, oxidative stress, and antioxidants: a review. *J. Biochem. Mol. Toxicol.* **17,** 24–38
115. Hebbel, R. P., Leung, A., and Mohandas, N. (1990) Oxidation-induced changes in microrheologic properties of the red blood cell membrane. *Blood* **76,** 1015–1020
116. Kaul, K., Tarr, J. M., Ahmad, S. I., Kohner, E. M., and Chibber, R. (2013) in *Diabetes. An Old Disease, a New Insight* (Ahmad, S., ed) pp. 1–11, Springer, New York
117. Harvey, R. M., Ogunniyi, A. D., Chen, A. Y., and Paton, J. C. (2011) Pneumolysin with low hemolytic activity confers an early growth advantage to *Streptococcus pneumoniae* in the blood. *Infect. Immun.* **79,** 4122–4130
118. Berry, A. M., Alexander, J. E., Mitchell, T. J., Andrew, P. W., Hansman, D., and Paton, J. C. (1995) Effect of defined point mutations in the pneumolysin gene on the virulence of *Streptococcus pneumoniae*. *Infect. Immun.* **63,** 1969–1974
119. Mitchell, T. J., Andrew, P. W., Saunders, F. K., Smith, A. N., and Boulnois, G. J. (1991) Complement activation and antibody binding by pneumolysin via a region of the toxin homologous to a human acute-phase protein. *Mol. Microbiol.* **5,** 1883–1888
120. Faure, P., Rossini, E., Wiernsperger, N., Richard, M. J., Favier, A., and Halimi, S. (1999) An insulin sensitizer improves the free radical defense system potential and insulin sensitivity in high fructose-fed rats. *Diabetes* **48,** 353–357
121. Rahbar, S., Natarajan, R., Yerneni, K., Scott, S., Gonzales, N., and Nadler, J. L. (2000) Evidence that pioglitazone, metformin and pentoxifylline are inhibitors of glycation. *Clin. Chim. Acta* **301,** 65–77
122. Beisswenger, P., and Ruggiero-Lopez, D. (2003) Metformin inhibition of glycation processes. *Diabetes Metab.* **29,** 6S95–96S103
123. Gallo, A., Ceolotto, G., Pinton, P., Iori, E., Murphy, E., Rutter, G. A., Rizzuto, R., Semplicini, A., and Avogaro, A. (2005) Metformin prevents glucose-induced protein kinase C-β2 activation in human umbilical vein

endothelial cells through an antioxidant mechanism. *Diabetes* **54,** 1123–1131
124. Gologan, P. (2013) *Red Blood Cell as an Elastic Probe: Interaction with Drugs and Toxins.* Ph.D. thesis, University of Exeter, Exeter, UK
125. Baker, N. A., Sept, D., Joseph, S., Holst, M. J., and McCammon, J. A. (2001) Electrostatics of nanosystems: application to microtubules and the ribosome. *Proc. Natl. Acad. Sci. U.S.A.* **98,** 10037–10041
126. Dolinsky, T. J., Czodrowski, P., Li, H., Nielsen, J. E., Jensen, J. H., Klebe, G., and Baker, N. A. (2007) PDB2PQR: expanding and upgrading automated preparation of biomolecular structures for molecular simulations. *Nucleic Acids Res.* **35,** W522–W525
127. DeLano, W. L. (2010) *The PyMOL Molecular Graphics System,* Version 1.6.0.0.0, Schroedinger, LLC, New York

Red Blood Cell Susceptibility to Pneumolysin: CORRELATION WITH MEMBRANE BIOCHEMICAL AND PHYSICAL PROPERTIES

Monika Bokori-Brown, Peter G. Petrov, Mawya A. Khafaji, Muhammad K. Mughal, Claire E. Naylor, Angela C. Shore, Kim M. Gooding, Francesco Casanova, Tim J. Mitchell, Richard W. Titball and C. Peter Winlove

J. Biol. Chem. 2016, 291:10210-10227.
doi: 10.1074/jbc.M115.691899 originally published online March 16, 2016
